Geological Field Trips

Società Geologica Italiana

ISPRA
Dipartimento per il
SERVIZIO GEOLOGICO D'ITALIA
Organo Cartografico dello Stato (legge n°68 del 2-2-1960)

2016
Vol. 8 (2.1)

INDEXED IN EMERGING SOURCES CITATION INDEX THOMSON REUTERS

ISSN: 2038-4947

The northernmost record of the Messinian salinity crisis (Piedmont basin, Italy)

Regional Commitee on Mediterranean Neogeone Stratigraphy Interim Colloquium – Torino, 2014

DOI: 10.3301/GFT.2016.03

GFT - *Geological Field Trips*

Periodico semestrale del Dipartimento per il Servizio Geologico d'Italia - ISPRA e della Società Geologica Italiana
Geol.F.Trips, Vol.**8** No.2.1 (2016), 58 pp., 27 figs. (DOI 10.3301/GFT.2016.03)

The northernmost record of the Messinian salinity crisis (Piedmont basin, Italy)

Regional Commitee on Mediterranean Neogeone Stratigraphy Interim Colloquium – Torino, 25-28 September 2014

Francesco Dela Pierre, Marcello Natalicchio, Francesca Lozar, Sabrina Bonetto, Giorgio Carnevale, Simona Cavagna, Simone Colombero, Mathia Sabino, Donata Violanti

Dipartimento di Scienze della Terra – Via Valperga Caluso, 35 – 10125 Torino (Italy)

Corresponding Author e-mail address: francesco.delapierre@unito.it

ISSN: 2038-4947 [online]

http://www.isprambiente.gov.it/it/pubblicazioni/periodici-tecnici/geological-field-trips

DOI: 10.3301/GFT.2016.03

INDEX

Information

Excursion notes

Itinerary

DOI: 10.3301/GFT.2016.03

Abstract

The aim of the field trip, regarding the southern (Langhe) and northern (Monferrato) part of the Tertiary Piedmont basin, is the description of the stratigraphical and sedimentological setting of the Messinian succession, which records the events of the Messinian salinity crisis (MSC). In the frame of this strongly debated scientific topic, the Piedmont basin is of particular interest, since it preserves the northernmost record of the MSC. The first two stops, located at the northernmost edge of the Langhe basin, allow the reconstruction of the lateral facies transition between a marginal (Stop 1) and a deeper sector (Stop 2) of the Messinian basin. The onset of the MSC is not marked here by an evaporite layer (as observed in other sectors of the MSC) but rather by peculiar laminated carbonate beds that are considered as the product of lithification of microbial mats dominated by sulphide-oxidizing bacteria (Stop 1). In the deeper sector of the basin (Stop 2) no sedimentological or lithological evidence can be observed at the MSC onset, which is recorded within a sequence of hemipelagic muds deposited on an oxygen-depleted sea bottom. The onset of the deposition of primary evaporites is strongly diachronous and more and more recent toward the deeper part of the basin. These primary evaporites consist of bottom-grown selenite and laminated microcrystalline gypsum ("cumulate gypsum"), which forms distinct beds regularly alternated to mudstone layers. These mudstone/gypsum couplets result from precession-controlled humid/arid climate oscillations with a periodicity of about 21 Ka. Primary evaporites are sharply followed, through a basin scale erosional unconformity, by resedimented and clastic gypsum facies, deposited in response of the tectonic deformation of the basin margins. The basal unconformity corresponds to the Messinian erosional surface, dated at 5.60 Ma. The Messinian succession ends with fluvio-deltaic terrigenous sediments, with continental vertebrate fossil assemblages, followed by brackish water marls which record the Lago Mare event at the end of the MSC, prior to the sudden return to normal marine conditions at the base of the Zanclean. In the northern margin of the Piedmont basin (Monferrato), the Messinian succession consists of chaotic deposits (huge gypsum blocks floating in a fine-grained matrix) which are the product of large scale mass wasting events related to the tectonic deformation of the Monferrato (Stop 3). The field trip ends in a quarry exposing a chaotic succession enclosing various types of methane-derived carbonate rocks (Stop 4). This succession is interpreted as the geological record of a Messinian submarine mud volcano.

Key words: Messinian salinity crisis, evaporites, gypsum, Piedmont basin

DOI: 10.3301/GFT.2016.03

Riassunto

Lo scopo principale dell'escursione, che attraversa la parte meridionale (Langhe) e settentrionale (Monferrato) del Bacino Piemontese, è la descrizione dell'assetto stratigrafico-sedimentologico della successione messiniana, che registra gli eventi connessi alla Crisi di salinità messiniana (CSM). Nell'ambito del dibattito scientifico sulla CSM, il Bacino Piemontese riveste particolare importanza, in quanto esso corrisponde al settore più settentrionale del Mediterraneo in cui sono registrate le evidenze della CSM stessa. La prima giornata si svolgerà nel margine settentrionale delle Langhe dove verranno osservate le transizioni di facies da un contesto marginale (Stop 1) ad uno più profondo (Stop 2). In quest'area, emerge che l'inizio della CSM non è contrassegnata dalla deposizione di evaporiti primarie (come osservato in altri settori del Mediterraneo) ma dalla comparsa di particolari livelli carbonatici laminati interpretati come il prodotto della litificazione di *microbial mats* dominate da batteri solfo-ossidanti (Stop 1). Nelle porzioni più distali del bacino (Stop 2) non si osserva invece alcuna evidenza sedimentologica dell'inizio di tale evento, che è registrato in una successione di peliti e marne deposte su un fondale marino carente di ossigeno (Stop 2). L'inizio della deposizione delle evaporiti primarie è fortemente diacrono, via via più recente verso i settori più profondi del bacino. Tali evaporiti sono rappresentate da banchi di gesso selenitico o microcristallino laminato ("gesso cumulitico") alternati in maniera ritmica a livelli pelitici, a formare cicli sedimentari di spessore variabile che registrerebbero oscillazioni climatiche arido (gesso)/umide (pelite) legate a variazioni della precessione terrestre, con una periodicità di circa 21 Ka. Le evaporiti primarie sono seguite da un complesso di evaporiti risedimentate deposte a seguito della deformazione tettonica dei margini del bacino. Tali sedimenti sono bordati alla base da una superficie di discontinuità (e dalla sua continuità correlativa) equivalente alla Messinian erosional surface (MES): quest'ultima, cui è assegnata un'età di 5.60 Ma, è stata riconosciuta in tutta l'area mediterranea. La successione si chiude con depositi terrigeni di ambiente fluvio-deltizio, che contengono ricche associazioni di vertebrati continentali, seguiti da depositi lacustri e salmastri che registrano l'evento Lago Mare, prima del ritorno a condizioni marine franche alla base dello Zancleano. La seconda giornata verrà dedicata alla successione messiniana affiorante nel Monferrato, al margine settentrionale del bacino (Stop 3); essa è costituita da depositi caotici (blocchi di gesso immersi in una matrice pelitica), che sono il risultato di imponenti fenomeni di risedimentazione in massa collegati alla deformazione tettonica del Monferrato. L'escursione termina con l'osservazione di peculiari masse carbonatiche metano-derivate (Stop 4) imballate in una successione argillosa, che sono interpretate come il record sedimentario di un vulcano di fango sottomarino di età messiniana.

Parole chiave: crisi di salinità messiniana, evaporiti, gesso, bacino piemontese

DOI: 10.3301/GFT.2016.03

Program

Day 1: the southern margin of the Piedmont basin

The starting point is Pollenzo (Cuneo Province), that can be easily reached by car from Torino following the A6 (Torino-Savona) motorway to Bra/Marene and then the A33 (Cuneo – Asti) motorway to the Cherasco station. To reach Stop 1A, follow the SP7 road to Pollenzo. At the roundabout turn on the right, up to the bridge on the Tanaro River and, immediately after it, turn to the left to the "Ristorante la Cascata" where a parking is available. From the restaurant, walk for ten minutes on the dirty road starting from the left of the restaurant and follow the indication to the "Spiaggia dei cristalli" (Crystal beach). To reach Stop 1B, from Ristorante la Cascata, drive to the roundabout, turn right and then left to the Restaurant Cin Cin Land. Park the car and walk on the dirty road for about 10 minutes to the Tanaro river banks. The section is entirely exposed along the left bank of the river. The transfer from Stop 1 (Pollenzo) to Stop 2 (Govone) requires about 30 min drive along the A33 to the exit of Costigliole-Govone; at the roundabout, turn to the right (direction Govone). Just before the bridge on the Tanaro river turn right and take the dirty road to "Lago Ario".

Be careful!: the turning can be dangerous: many trucks usually travel on the main road!
Park the car and walk along the right bank of the Tanaro river.

Day 2: the northern margin of the Piedmont basin

To reach the Cava di Murisengo (Stop 3) from Asti (30 min drive), take the SS 457 to Castell'Alfero (direction: Casale Monferrato) and then the SP 22 to Murisengo. **Warning**: This Stop is located in an active gypsum quarry and can be visited only with the agreement and accompaniment of the owner. Contact the owner at: tecnico@estrazionegesso.com. The transfer to Stop (4) requires 30 min drive along the SP500 (direction Torino) to Cavagnolo. At the traffic light, turn right to Verrua Savoia-Crescentino and at Rocca turn right following the indication to "Rocca di Verrua Savoia". Following the dirty road, reach the parking and take the path on the right. After ten minute walk, you will meet the explanatory panel of this newly established geosite, showing the geological history of the Verrua Savoia mud volcano. The trip continues downward through the abandoned Verrua-Savoia quarry.

DOI: 10.3301/GFT.2016.03

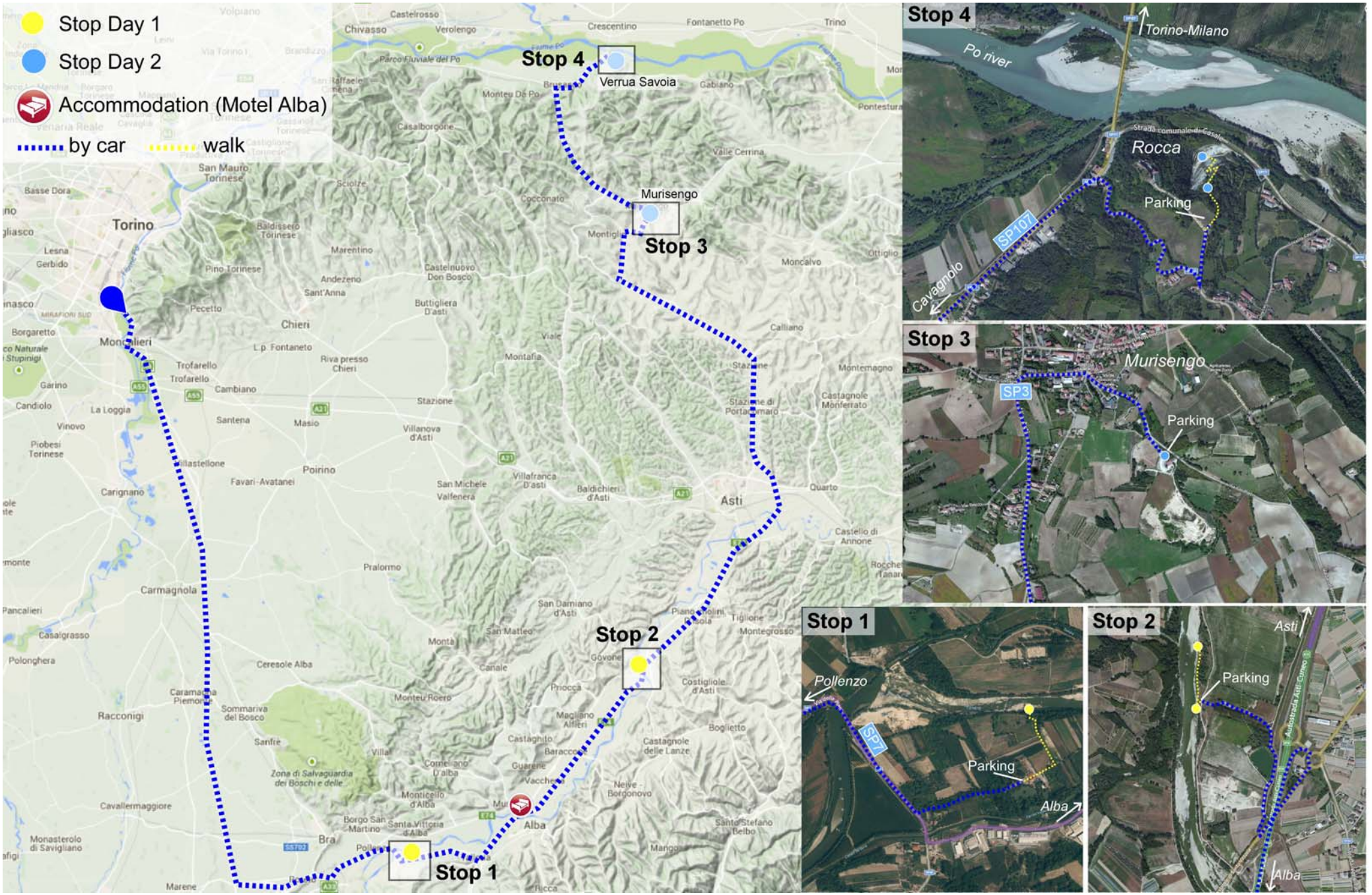

Fig. 1 - Itinerary of the field trip (Google Earth). The insets on the right show the satellite map of the four stops (Bing map).

DOI: 10.3301/GFT.2016.03

Safety

The itinerary is located in the hilly country of Piedmont at an average altitude of 300 m. The best seasons for the visit are spring and autumn: winter and summer can be very cold or very hot, respectively. Avoid to schedule the visit after days of heavy rain: the stops located on the bank of the Tanaro river can be very dangerous if the level of the water is high.
Rain or light mountain boots are strongly needed: in most of the outcrops mud is present. Sun glasses, a sun–tan lotion and a protective lotion against mosquitoes are strongly recommended, as well as waterproof and wind resistant clothing.

Hospitals

Bra - Ospedale Spirito Santo - Via Vittorio Emanuele 3 – 12042 Bra (CN). Tel: 0172 420111
Alba - Ospedale San Lazzaro - Via Pierino Belli, 26 – 12051 Alba (CN). Tel: 0173 366219
Asti - Ospedale Civile - Corso Dante Alighieri 202 – 14100 Asti. Tel: 0141 481111

Emergency Contact numbers

113 – Polizia di Stato
115 – Fire-fighters
118 – First Aid

Accomodation

Motel Alba - Corso Asti, 5 – 12051 Alba (CN).
Tel: 0173 363251

Maps

Carta Geologica d'Italia 1:100.000, Sheet 69 "Asti"
Carta Geologica d'Italia 1:50.000, Sheet 157 "Trino"

Other useful addresses

Museo civico archeologico e di Scienze Naturali Federico Eusebio Via V. Emanuele 19, Alba (CN).
Tel: 0173 292473

http://www.comune.alba.cn.it/index.php?option=com_content&view=article&id=58:museo&catid=37:museo&Itemid=97

Museo Civico Craveri di Storia Naturale - Via Craveri 15, Bra (CN). Tel: 0172 412010
http://www.museocraveri.it

DOI: 10.3301/GFT.2016.03

1. Introduction

During the Messinian, the Mediterranean basin was transformed in one of the largest salina basin of the Earth history (e.g. Hsü et al., 1973; Cita et al., 1978). The progressive reduction of the connections with the Atlantic Ocean modified seawater chemistry and salinity, culminating with the establishment of a hypersaline water body. This event, known as the Messinian salinity crisis (MSC) occurred in a brief time interval (about 700 ka; Krijgsman et al., 1999; Manzi et al., 2013) and severely impacted on both terrestrial and marine ecosystems. Its sedimentary products are more than 1 million of Km^3 of evaporites (gypsum, anhydrite, halite) interbedded between deep water marine sediments and deposited in a mosaic of different sub-basins inherited from a highly diversified and complex geodynamic settings (e.g. Rouchy & Caruso, 2006; Ryan, 2009) (Fig. 2).
The integration of cyclostratigraphic, bio- and magnetostratigraphic data with facies analysis and physical stratigraphy from different onshore Mediterranean basins has provided a detailed chronostratigraphic framework of the MSC events (Fig. 3), that is now largely accepted by the scientific community (CIESM, 2008; Roveri et al., 2014).

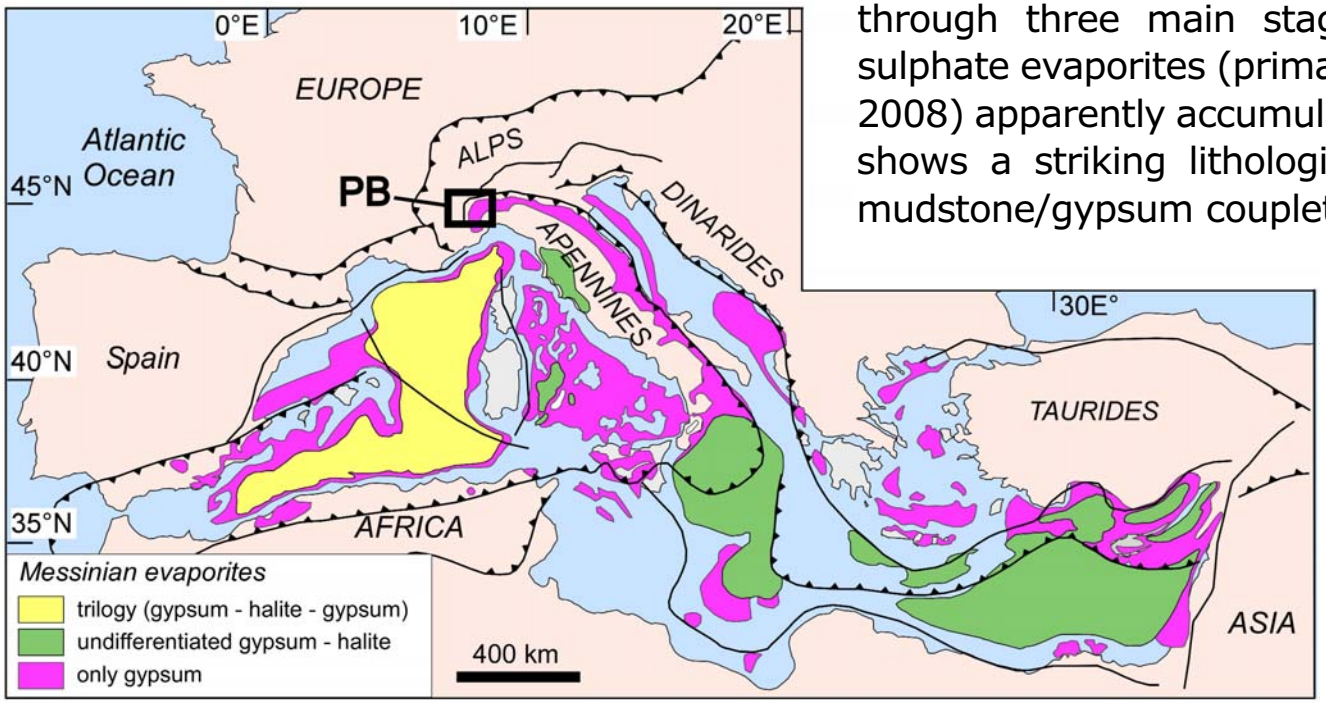

Fig. 2 - Distribution of the Messinian evaporites in the Mediterranean (modified from Manzi et al., 2013). **PB:** Piedmont basin.

According to these detailed reconstructions, the MSC evolved through three main stages. During **stage 1 (5.97-5.60 Ma)** sulphate evaporites (primary lower gypsum unit - PLG; Roveri et al., 2008) apparently accumulated in shallow peripheral basins. The PLG shows a striking lithologic cyclicity, marked by the repetition of mudstone/gypsum couplets reflecting precession-driven humid/arid climate oscillations. In this time interval, deep basinal areas experienced deposition of organic-rich shales interbedded to carbonate-rich beds (Manzi et al., 2007; De Lange & Krijgsman 2010; Dela Pierre et al.,

DOI: 10.3301/GFT.2016.03

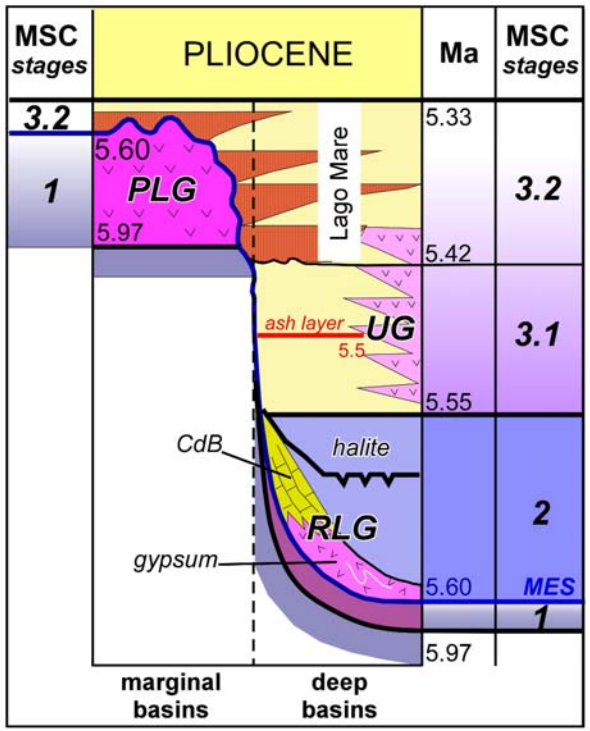

Fig. 3 – MSC chronostratigraphy (modified from CIESM, 2008; Manzi et al., 2013). **CdB:** calcare di base; **PLG:** primary lower gypsum unit; **RLG:** resedimented lower gypsum unit; **UG:** upper gypsum; **MES:** Messinian erosional surface; **MSC:** Messinian salinity crisis.

2011; 2012). During **stage 2 (5.60-5.55 Ma; *acme of the MSC*)** peripheral basins experienced subaerial exposure and erosion, with the development of the Messinian erosional surface (MES). The correlative conformity of the MES can be traced, in the deep basins, at the base of clastic and resedimented evaporites (resedimented lower gypsum unit - RLG; Roveri et al., 2008) sourced by the dismantlement of the PLG unit. The primary evaporites of this stage are mostly represented by halite and K-Mg salts, that rapidly filled some of the sub-basins, as testified by the clear shallowing upward trend and by the presence of subaerial exposure surfaces (Lugli et al., 1999). During **stage 3** (**5.55 - 5.33 Ma)** a new evaporite unit (upper gypsum unit; see Manzi et al., 2009) precipitated in shallow sub-basins in the Southern and Eastern Mediterranean from waters dominated by important continental input. Evaporite-free clastic sediments deposited in the Western and Northern Mediterranean sub-basins. The presence of brackish to fresh water "Lago Mare" fauna and flora with Paratethyan affinity in stage 3 deposits (e.g. Orsazg Sperber, 2006; Rouchy & Caruso, 2006; Roveri et al., 2014) indicates the dilution of the surface waters related to hydrological modifications in response to significant palaeoclimate and palaeogeographical changes. However, marine stenohaline fishes have been reported from several localities (Carnevale et al., 2006; 2008), posing the question of the possible connection between the Mediterranean and the Atlantic ocean during the final stage of the MSC. The reestablishment of fully marine conditions at the base of the Zanclean (5.33 Ma) definitely marks the end of the MSC.

The Messinian succession of the Piedmont basin was one of the reference sections for the interpretation of the complex MSC events in the years immediately following the formulation of the deep desiccated basin model (Sturani, 1973; Cita et al., 1978). However, in recent years it has been neglected, despite its study may certainly provide an important contribution to understanding the MSC events at the northern Mediterranean edge. The aim of this field trip is to discuss the recent stratigraphical, sedimentological, palaeontological, and geochemical data (Colombero et al., 2013; 2014; Dela Pierre et al., 2011; 2012; 2014; Lozar et al., 2010; Natalicchio et al., 2012; 2013; 2014; Violanti et al., 2009; 2011; 2013) on the MSC events recorded in the Piedmont basin.

DOI: 10.3301/GFT.2016.03

2. Geological Setting

The Piedmont basin (PB), located on the inner side of SW Alps arc (Fig. 4A), is filled with Upper Eocene to Messinian sediments that cover a complex tectonic wedge of Alpine, Ligurian and Adria units juxtaposed in response of the collision between Europe and Adria plates (mesoalpine collisional events) (Roure et al. 1996; Bertotti & Mosca, 2009; Mosca et al., 2009; Rossi et al., 2009). These Cenozoic sediments are presently exposed in the southern (Langhe) and in the northern (Torino Hill - Monferrato arc) sectors of the basin (Fig. 4A). The relationships between the two outcropping belts are masked by Pliocene-Quaternary deposits of the Savigliano and Alessandria basins, but are well imaged by seismic profiles (Bertotti & Mosca, 2009). Outcrop and seismic data show that the Late Eocene-Oligocene succession consists of continental and shallow marine deposits, followed by Upper Oligocene-Lower Miocene turbidites (see Rossi et al., 2009). Since the late Burdigalian, a more regular

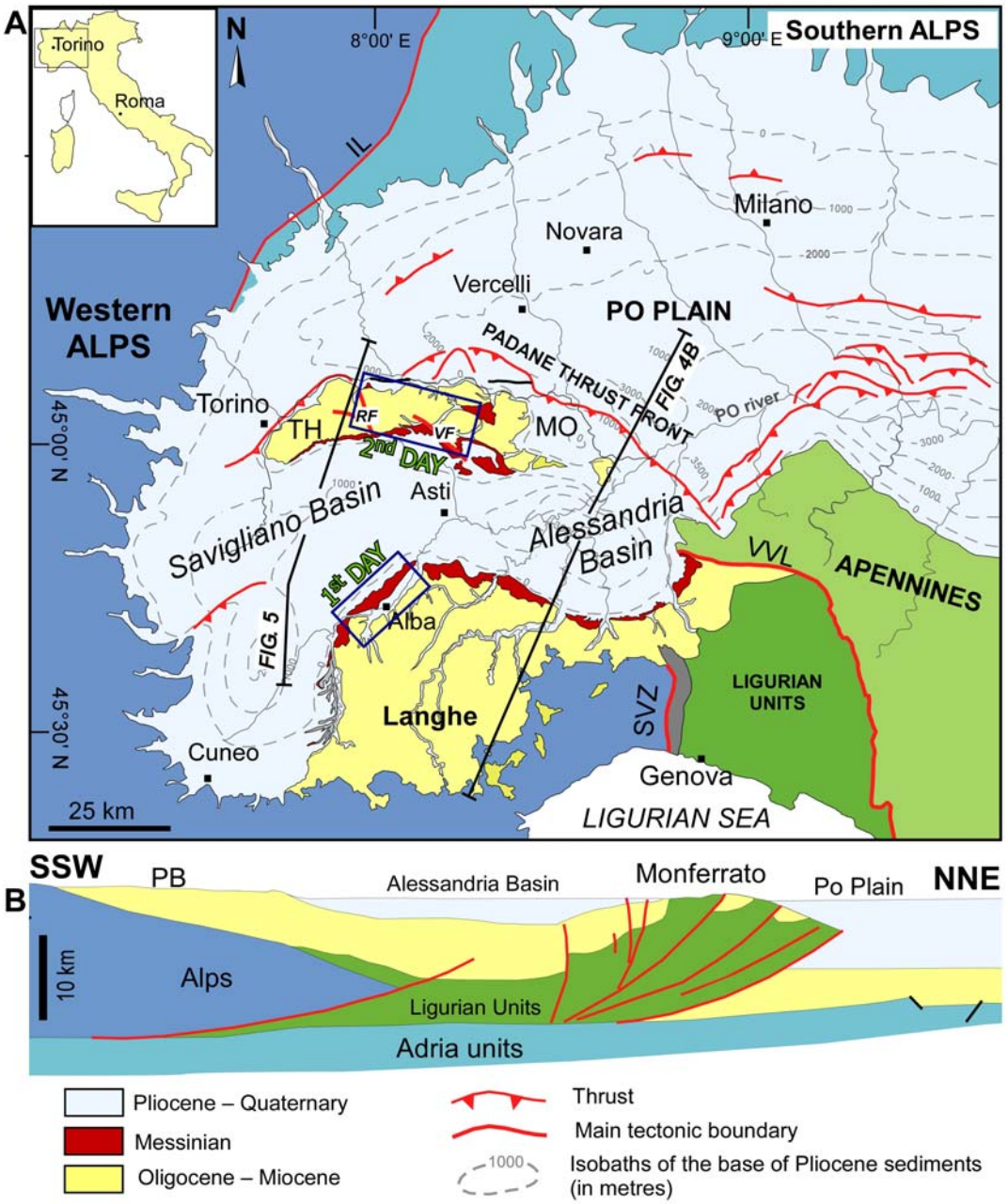

Fig. 4 – **A)** Structural sketch map of the Piedmont basin (modified from Bigi et al., 1990); **TH:** Torino Hill; **MO:** Monferrato; **VVL:** Villalvernia–Varzi line; **IL:** Insubric line; **RF:** Rio Freddo fault; **VF:** Villadeati fault; **SVZ:** Sestri-Voltaggio zone. **B)** Regional section in a NE-SW direction (modified from Mosca et al., 2009).

DOI: 10.3301/GFT.2016.03

physiography was established and the PB behaved as a single large wedge-top basin, bounded to the north by the uplifted Monferrato arc. The structural setting of this last basin is complicated by NW-SE transpressive faults (Clari et al., 1995; Piana, 2000), the most important of which are the Rio Freddo and the Villadeati fault zones (Fig. 4A). These structures affected deposition of the Cenozoic succession, that was deposited in fault-bounded subsiding sub-basins separated by intervening structural highs (Dela Pierre et al., 2003).

The progressive uplift of the southern part of the PB and its tilting towards the north occurred since the Middle Miocene (Langhian) (Bertotti & Mosca, 2009; Mosca et al., 2009). During the Late Miocene, the north-verging Apennine tectonics involved the Torino Hill area. The N-S crustal shortening was accommodated by further uplift of the southern parts of the PB and by the establishment of two major subsiding depocentres (Savigliano and Alessandria basins), developed in a piggy-back basin bordered by the Torino Hill –Monferrato tectonic arc (Rossi et al., 2009; Fig. 4B). This last sector is eventually overthrust to the north onto the Po Plain foredeep, along the Late Neogene to Quaternary Padane thrust front that corresponds to the westward prolongation of the more external Apennine thrusts.

Summarizing, Messinian strata were deposited in a wide wedge top basin: the shallow marginal zones are presently exposed in the southern (Langhe) and northern (Torino Hill-Monferrato) sectors, whereas the depocentral zones are buried below Pliocene-Quaternary sediments (Savigliano and Alessandria basins) (Fig. 5).

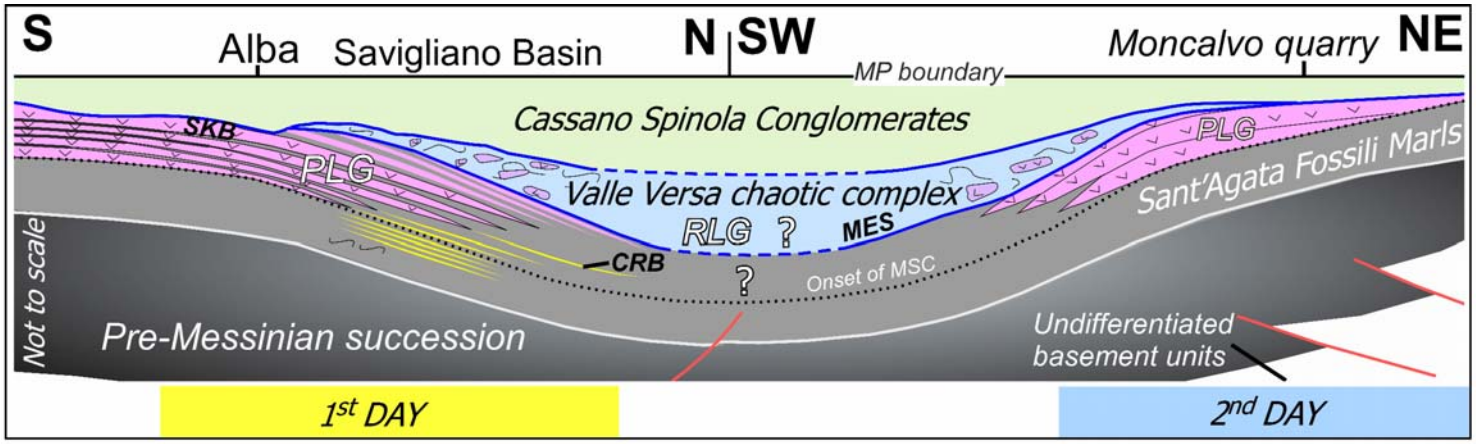

Fig. 5 – Schematic cross section, flattened at the base of the Pliocene, showing the relationships among the Messinian units. **PLG:** primary lower gypsum unit; **RLG:** resedimented lower gypsum unit; **SKB:** Sturani key-bed; **CRB:** carbonate-rich beds; **MES:** Messinian erosional surface. Location in Fig. 4A (from Dela Pierre et al., 2011).

DOI: 10.3301/GFT.2016.03

3. Stratigraphy of the Messinian sediments

In the PB, the Messinian succession starts with outer shelf to slope muddy sediments referred to as the Sant'Agata Fossili marls (Tortonian-lower Messinian) (Fig. 5) that record progressively more restricted conditions heralding the onset of the MSC (Sturani, 1973; Sturani & Sampò, 1973). This unit displays a precession-related cyclic stacking pattern, evidenced by the rhythmic repetition of shale/marl couplets (Lozar et al., 2010; Dela Pierre et al., 2011; Violanti et al., 2013) and is followed, at the basin margins, by primary sulphate evaporites referred to as the primary lower gypsum unit (PLG; Roveri et al., 2008) (Fig. 5). The latter was deposited during stage 1 of the MSC and shows the same precession-driven lithologic cyclicity, represented by shale/gypsum couplets (Dela Pierre et al., 2011) as elsewhere in the Mediterranean (e.g. Krijgsman et al., 1999; 2001; Lugli et al., 2010; Manzi et al., 2013). No *in situ* primary evaporites are documented in the depocentral zones, but seismic data show that their time equivalent sediments are represented by shales (Irace et al., 2010).
The PLG unit is followed by resedimented and chaotic evaporites, referred to as the Valle Versa chaotic complex (Dela Pierre et al., 2003; 2007); this unit is equivalent of the resedimented lower gypsum unit (*RLG;* Roveri et al., 2008) deposited during the second MSC stage (5.60-5.55 Ma) (Dela Pierre et al., 2011). The Valle Versa chaotic complex is followed by fluvio-deltaic and lacustrine deposits (Cassano Spinola conglomerates) recording the third MSC stage (5.55-5.33 Ma) and showing at the base another erosional unconformity, cutting the MES at the basin margins (Fig. 5). Deposition of Zanclean marine clays and marls (Argille Azzurre Formation) marks the end of the salinity crisis at 5.33 Ma (Violanti et al., 2011) as in all the other Mediterranean sub-basins (Fig. 5).

DOI: 10.3301/GFT.2016.03

Day 1 - The southern margin of the Piedmont basin

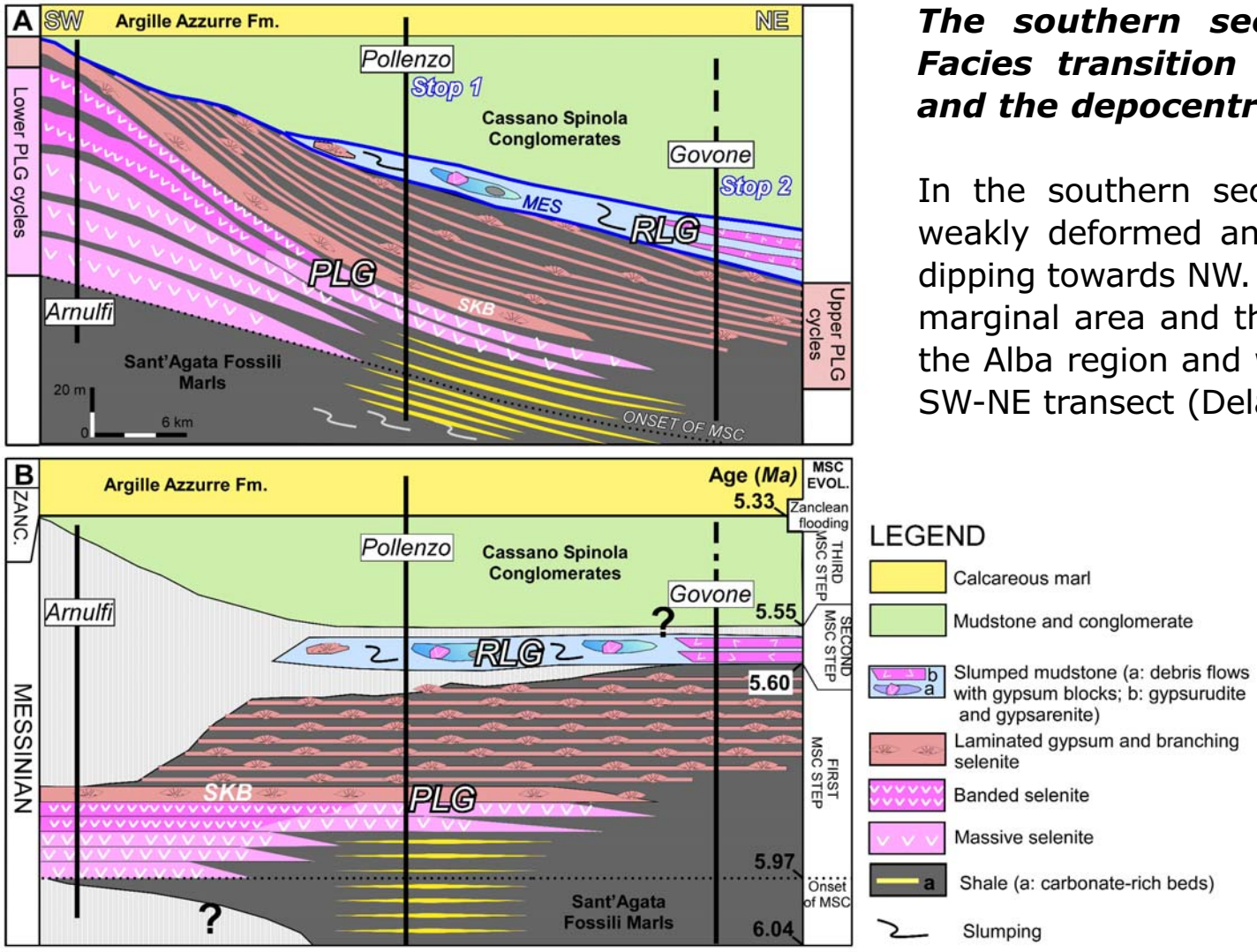

Fig. 6 – Stratigraphic model of the MSC record of Alba. **A)** cross section flattened at the base of the Pliocene. **B)** chronostratigraphic scheme. **PLG:** primary lower gypsum; **RLG:** resedimented lower gypsum. **SKB:** Sturani key-bed; **MES:** Messinian erosional surface (modified from Dela Pierre et al., 2011).

The southern sector of the Piedmont basin. Facies transition between the shallow margin and the depocentre.

In the southern sector of the PB, the succession is weakly deformed and arranged in a monocline gently dipping towards NW. The transition between the shallow marginal area and the buried depocentre is exposed in the Alba region and was reconstructed in detail along a SW-NE transect (Dela Pierre et al., 2011) (Figs. 6A, B).

1.1 The PLG unit (1st MSC stage)
On the basin margin (Arnulfi section, located to the SW of the proposed itinerary) six PLG cycles were recognised, overlying the pre-evaporitic Sant'Agata Fossili marls (Figs. 6, 7). Gypsum beds composing the lower three cycles, up to 10 m thick, consist of massive selenite and are made up of decimetre-sized vertically arranged twinned crystals whose size is rather constant through the beds. The fourth and fifth gypsum beds consists of banded selenite, i.e parallel layers of

DOI: 10.3301/GFT.2016.03

Fig. 7 – Arnulfi section (not observed in this field trip). Panoramic view of the upper part. The thirds, fourth and fifth gypsum beds are visible under the trees. The sixth gypsum bed (Sturani key-bed: **SKB**) is also recognisable.

twinned crystals having the same size (5-10 cm), separated by thin clayey beds. This vertical facies transition suggests the progressive increase of brine concentration, due to continuous evaporation (Dela Pierre et al., 2011). A sharp facies change is recorded by the 6th bed, about 10 m thick (Fig. 8A). This layer represents a distinct marker bed that can be physically correlated and mapped throughout most of the PB, allowing detailed physical-stratigraphic correlations. It was named Sturani key-bed (SKB) in memory of Carlo Sturani, the scientist who first provided a comprehensive study of the Messinian succession of the basin (Sturani, 1973; 1976). This marker bed is characterised by centimetre-to metre size flat conical structure growing in a matrix of cumulate gypsum that consists of the regular alternation of mm thick clay/gypsum laminae. Gypsum laminae are composed of tiny (10-20 μm) prismatic single crystals or twins that do not show any preferential orientation but are randomly distributed on the lamina surface: this is commonly observed in cumulate deposits, made up of crystals formed at the water/air interface (or in the water column) and settled down to the bottom. The cones are formed by millimetre-to centimetre-sized selenite crystals with horizontal or slightly inclined long axes. These features were at first interpreted as early diagenetic products resulting from the displacive growth of coarse-grained selenite masses within the laminated matrix (Sturani, 1973). However, the re-examination of these structures have shown that they are comparable to the branching selenite facies, described by Lugli et al. (2010) in the Mediterranean PLG deposits. These authors have suggested that the branching selenite appears

DOI: 10.3301/GFT.2016.03

from the 6th PLG cycle (*i.e.* at around 5.87 Ma; Manzi et al., 2013) at the Mediterranean scale, providing a tool for bed by bed correlation between sections located thousands of km apart.
The synchronous appearance of the branching selenite would result from a basin-wide hydrologic change, concomitant with the input of Atlantic water in the Mediterranean that is suggested by the shift of Sr isotope values contrasting with the stronger continental signature of the lower cycles (Lugli et al., 2007). No Sr isotope data are available for the PB; however, such an increase of the oceanic water input in the same time interval is supported by the findings of marine stenohaline fishes below and above the SKB (Sturani, 1973; Gaudant & Cavallo, 2008).
A different succession was observed in the Pollenzo section **(Stop 1)** located to the NE, i.e. towards the deeper part of the basin (Fig. 6). Here only two thin gypsum beds (massive selenite) are present below the SKB, overlying a cyclic succession of laminated dark-grey shales, marls and carbonate-rich beds that belongs, from the lithostratigraphic point of view, to the Sant'Agata Fossili marls. Due to their position with respect to the Sturani key-bed (PLG6) it was proposed that the two gypsum beds underlying the SKB correlates with cycles PLG5 and PLG4; therefore, the uppermost three cycles of the Sant'Agata Fossili marls are time equivalent of the lower three PLG cycles deposited in marginal settings (Dela Pierre et al., 2011). This correlation is strongly supported by biomagnetostratigraphic data, indicating that the onset of the MSC should be placed at Pollenzo three lithologic cycles below the first local gypsum bed, in correspondence of the peak abundance of the calcareous nannofossil *Sphenolithus abies* (Lozar et al., 2010; Violanti et al., 2013) (see below). This means that the onset of gypsum deposition in the PB is diachronous over a lateral distance of few kilometres and is progressively younger basinward.
Above the SKB, seven cycles can be recognised at Pollenzo characterised by the branching selenite facies. The gypsum beds are similar to the underlying SKB, except for their reduced thickness (up to 2 m) and the greater amount of clayey fraction (Fig 8B). Some layers (Pg5) are laterally discontinuous and formed by decimetre-sized cones floating within a matrix of gypsiferous silty mudstones. The higher clayey fraction in these upper PLG cycles may be indicative of a more effective continental runoff from neighbouring continental areas, suggesting the influence of humid climate conditions at the end of the first MSC stage (Dela Pierre et al., 2011).

In the Govone section (**Stop 2**), located in more distal settings, the PLG unit comprises nine lithologic cycles (Fig. 6). No massive or banded selenite layers are present and the SKB could not be recognised. Gypsum beds, up to 3 m thick, are made up of laminated gypsiferous silty mudstone consisting of interbeds of gypsum-free and

DOI: 10.3301/GFT.2016.03

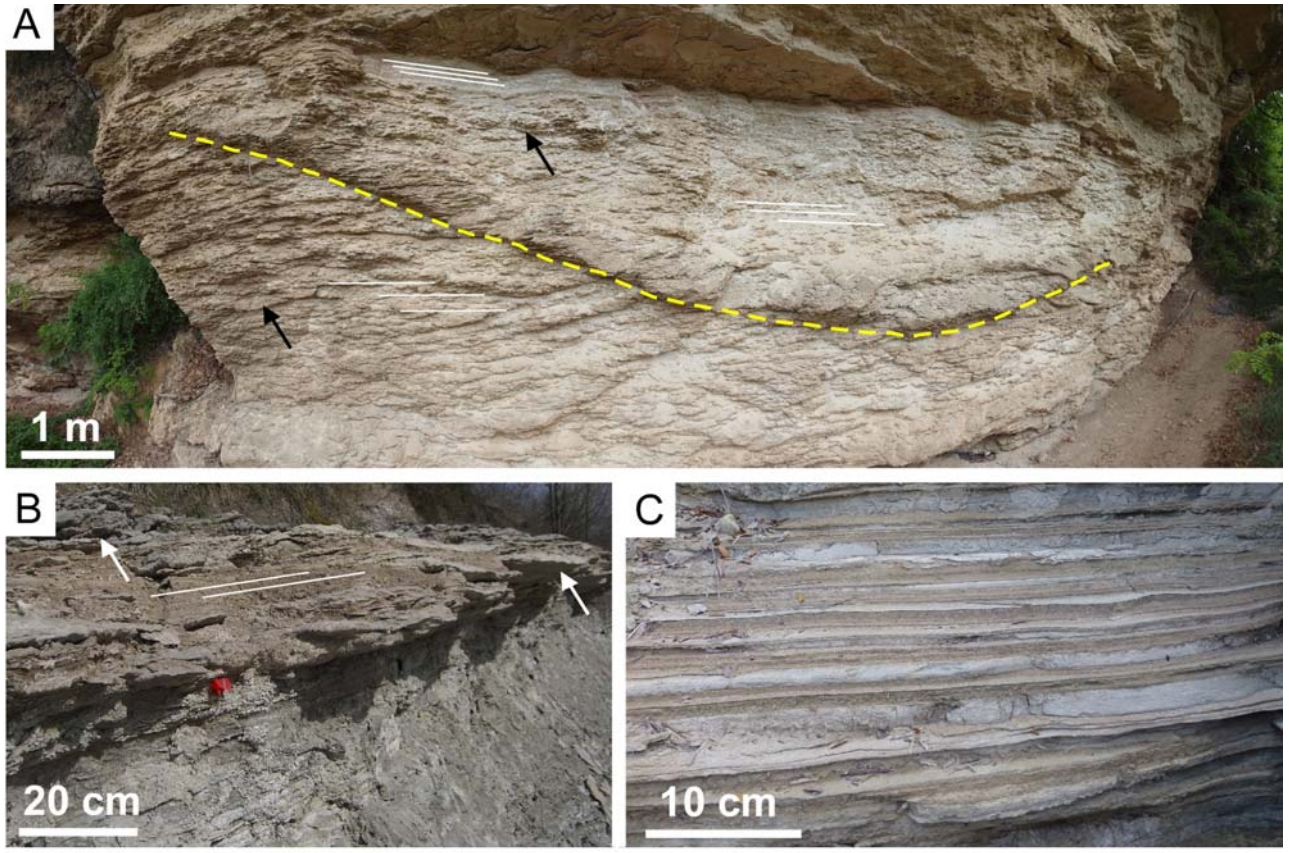

Fig. 8 – **A)** The Sturani key bed (Arnulfi section): note the "nodular" aspect, given by coalescent conical structures (arrows) growing in a laminated matrix (white lines) and the "arm" of large asymmetric cone (yellow dotted line). **B)** Outcrop view of the gypsum bed above the SKB, consisting of flat conical features (arrows) within a laminated matrix (white lines) (cycle Pg4, Pollenzo section). **C)** Gypsiferous silty mudstones (cycle Gg2, Govone section); note the alternation of brownish gypsum-rich and whitish gypsum-free layers.

gypsum-rich mudstone layers and laminae. The latter contains tiny, randomly oriented gypsum crystals, settled down from the water column and floating in muddy matrix (Fig. 8C).
The boundary with the gypsum-free mudstone layers is transitional through the gradual increase in the number of gypsum crystals. In some layers scattered flat and radial conical structures ("*padellini*") composed of interlocked mm- to cm-across prismatic selenite crystals are present. They can be interpreted as poorly developed branching selenite structures, whose growth was hampered by mud deposition. Slumped intervals and thin layers of clastic gypsum are also present.
As at Pollenzo, the PLG unit overlies the Sant'Agata Fossili marls that display a well-developed lithologic cyclicity. Biomagnetostratigraphic analyses suggest that the onset of the MSC should be placed in the upper part of this unit, 7 lithologic cycles below the first local gypsum bed (see below). Consequently, a total of 16 cycles deposited during the first MSC stage is preserved in this section (Fig. 6).

DOI: 10.3301/GFT.2016.03

1.2 The Post PLG sediments (2nd and 3rd MSC stages)

On the southern basin margin, primary evaporites are followed by slumped mudstone enclosing metre-sized blocks of gypsum similar to those composing the upper PLG cycles, and (locally) of carbonate rocks (presently under study). This unit (Valle Versa chaotic complex) was deposited during the second MSC stage, and its basal surface is correlated with the Messinian erosional surface (MES). At the basin margin (Pollenzo) it is 5 m thick, becoming thicker toward the NE. *i.e.* toward the depocentre. At Govone it is about 20 m thick and includes layers of clastic gypsum (gypsarenite and gypsrudite) together with slumped and chaotic intervals. Seismic data show that in the buried depocentre (Savigliano and Alessandria basin) the chaotic unit reaches a thickness of 400 m. Here no primary gypsum facies have been recognised and the chaotic unit sharply overlays a prevalent muddy succession. The third MSC stage is recorded by the Cassano Spinola conglomerates (Dela Pierre et al., 2011). This terrigenous unit consists of fluvio-deltaic deposits, followed by marls with brackish water fossil assemblages pertaining to the Lago Mare biofacies (see below). The basal surface of the Cassano Spinola conglomerates is a sharp erosional surface that cuts progressively towards the basin margins (i.e. towards the SW) (Fig. 6).

STOP 1 - The Pollenzo section

In this section (Fig. 9), located along the Tanaro River, a complete Messinian succession is exposed, comprising the Sant'Agata Fossili marls, the primary lower gypsum, the Valle Versa chaotic complex (= resedimented lower gypsum unit), the Cassano Spinola conglomerates and the Zanclean Argille Azzurre Formation.

Stop 1A - The Crystal beach: panoramic view of the section and the Sturani key-bed

In this Stop it is possible to observe a panoramic view of the Pollenzo section on the opposite bank of the river (Fig. 10), the second local gypsum bed (Pg2) and the Sturani key-bed (Pg3). The second gypsum bed (PLG5) is about 1 m thick and is composed of vertically oriented dm-sized twinned crystals that contain in the re-entrant angles clay floccules and rare filaments. At the base, conical structures composed of larger crystals placed at low angles with respect to the bedding planes can be observed. At the top, the gypsum crystals are locally surrounded by a carbonate crust (Fig. 11A).

The Sturani key-bed (PLG6) can be observed on a cut parallel to bedding. The most prominent features are flattened cones (branching selenite), up to several metres in size, that are composed of clusters of smaller-sized cones, in turn formed by millimetre to centimetre-sized selenite crystals with their long axis inclined or

DOI: 10.3301/GFT.2016.03

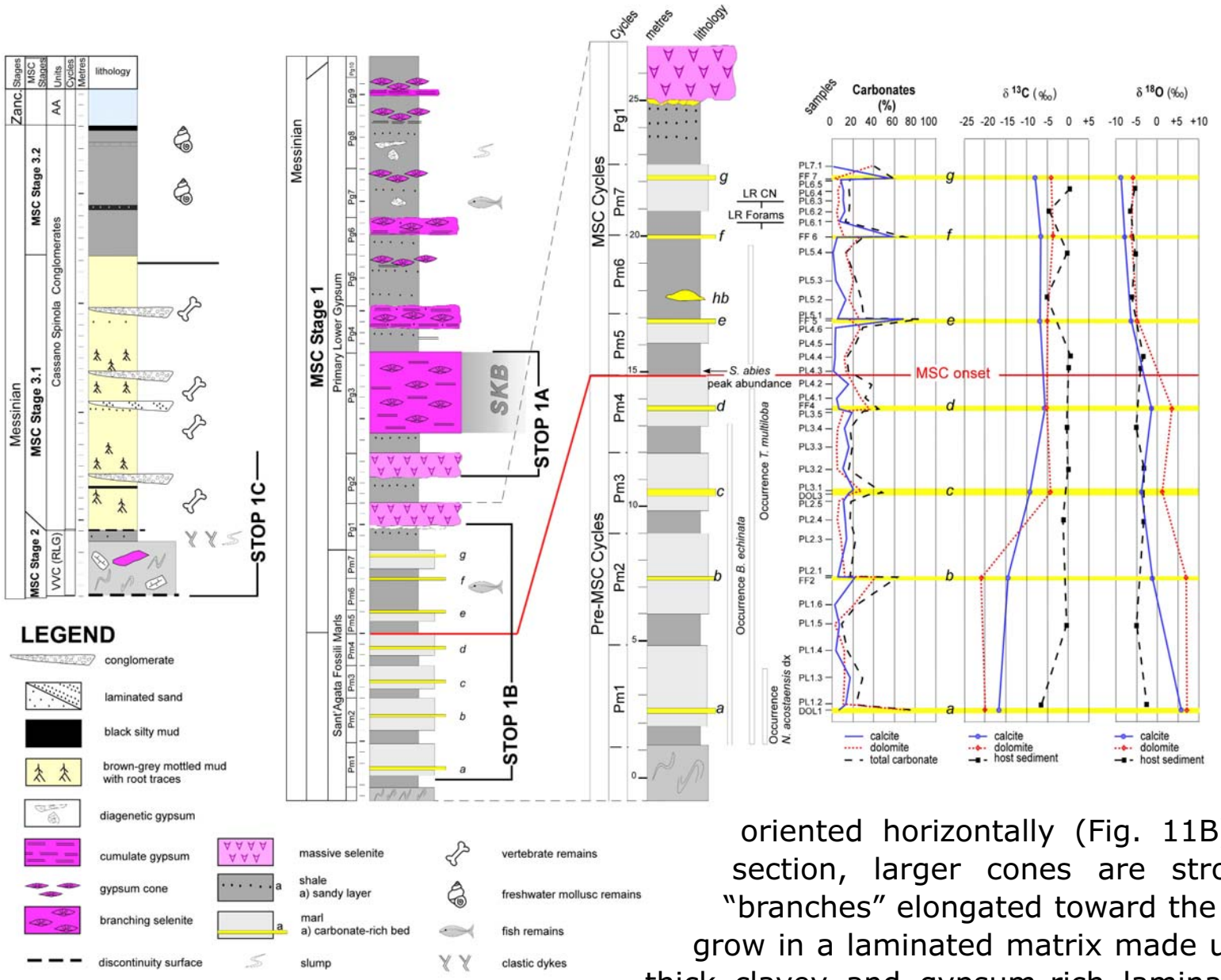

Fig. 9 – The Pollenzo section above the slump and detail of the upper part of the Sant'Agata Fossili marls (right). Inductively coupled plasma (ICP) data (total carbonates, dolomite and calcite) and stable isotope data of pre-MSC and MSC cycles are shown. **SKB:** Sturani key-bed; **RLG:** resedimented lower gypsum unit; **VVC:** Valle Versa chaotic complex; **AA:** Argille Azzurre Formation; **hb:** hemi-ellipsoidal body. Chrono-biostratigraphic data and distribution of foraminifers and calcareous nannofossils are from Violanti et al., 2013.

oriented horizontally (Fig. 11B). When observed in cross section, larger cones are strongly asymmetric, forming "branches" elongated toward the north (Fig. 12A). The cones grow in a laminated matrix made up of the alternation of mm-thick clayey and gypsum-rich laminae (cumulate gypsum) (Fig. 12B). Gypsum laminae are composed of tiny (10-20 μm) crystals. Within clay-rich laminae, gypsum crystals are less abundant. Dragonfly larvae and land plant debris, concentrated in the terrigenous laminae, were observed and interpreted as transported from neighbouring continental areas.

DOI: 10.3301/GFT.2016.03

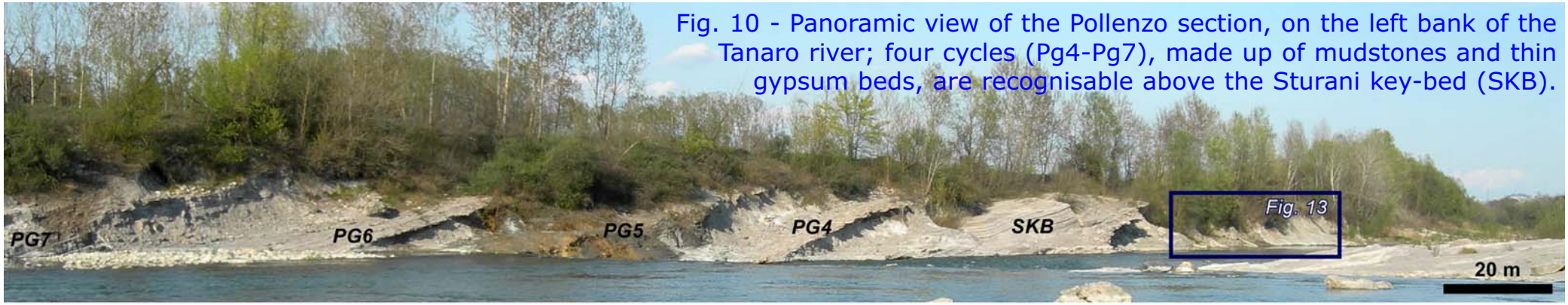

Fig. 10 - Panoramic view of the Pollenzo section, on the left bank of the Tanaro river; four cycles (Pg4-Pg7), made up of mudstones and thin gypsum beds, are recognisable above the Sturani key-bed (SKB).

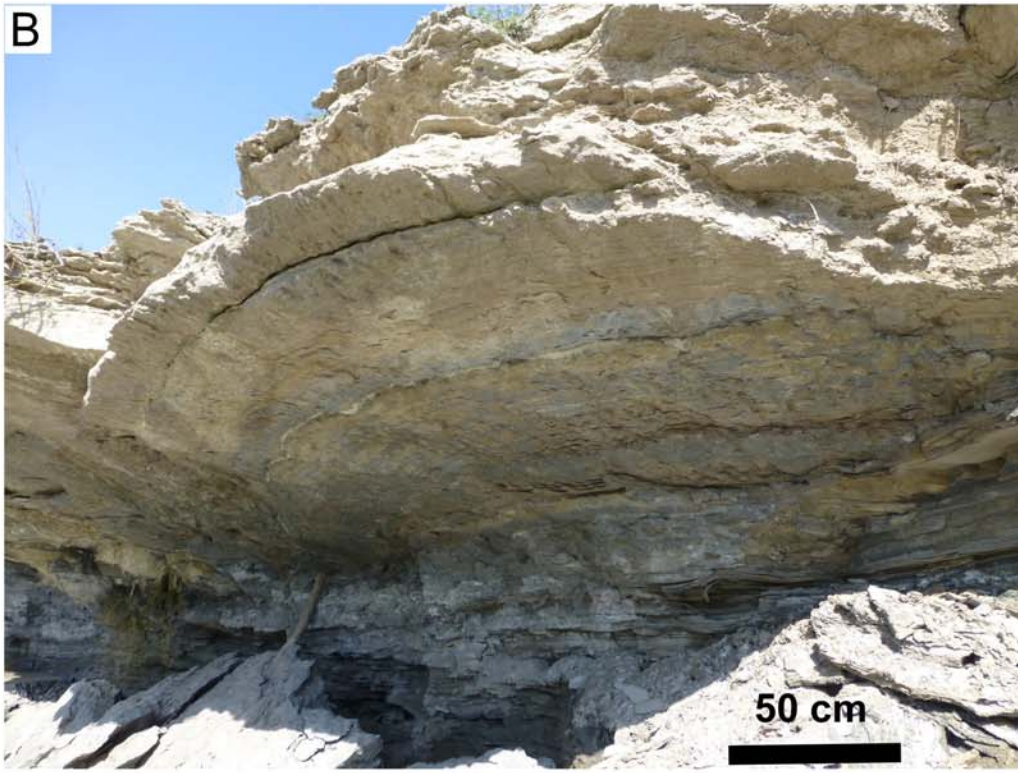

Fig. 11 - **A)** Conical structures (nucleation cones) at the base of the bottom-grown selenite layer of cycle Pg2. **B)** Metre-sized flat conical feature (branching selenite) at the base of the Sturani key-bed.

DOI: 10.3301/GFT.2016.03

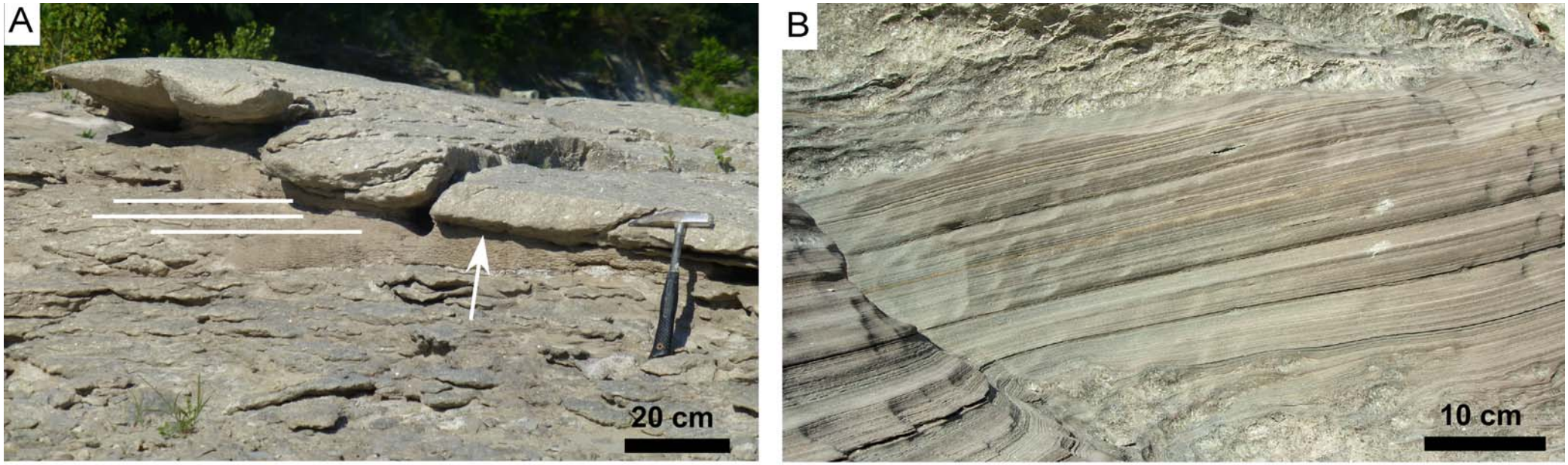

Fig. 12 - **A)** The Sturani key-Bed. Note the flattened cones and the laminated matrix (white lines). The arrow indicates a m-sized structure composed of small cones. **B)** Laminated gypsum.

Stop 1B - The upper part of the Sant'Agata Fossili marls and the transition to the PLG unit

The upper part of the Sant'Agata Fossili marls is exposed for about 130 m on the opposite bank of the river. A 80 m thick slumped interval allows to separate the section into two parts. The *lower part* shows a distinctive lithologic cyclicity: seven cycles, about 3 m thick, and composed of shales and homogeneous marls, were recognised. Fossil content of marly beds consists of benthic and planktonic foraminifers, calcareous nannofossils, bivalves (*Propeamussium* spp.and *Cuspidaria spp.*), nassarid gastropods, pteropods (*Cavolinia* sp., *Clio* sp., *Limacina* spp.) and land plant debris. The remains of epi- and bathypelagic fishes (clupeids and myctophids) have been found in the shaly layers (Gaudant & Cavallo, 2008), besides foraminifers and nannofossils. Calcareous plankton assemblages are indicative of the *Globorotalia conomiozea* Zone (Iaccarino, 1985) and the MNN11b/c Zone of Raffi et al. (2003), documenting the Messinian age. Foraminiferal assemblages indicate a change from open marine conditions to a more restricted, probably shallower and

DOI: 10.3301/GFT.2016.03

poorly oxygenated basin. The sediments are overlaid by the slumped interval, in which beds are intensively folded and deformed. Above the slump (*upper part),* the lithologic cyclicity is enhanced by the rhythmic alternation of carbonate-rich beds, easily recognisable for their whitish colour (Fig. 13). Seven cycles (Pm1-Pm7), composed of a basal shaly layer followed by a marly bed were recognised, each one including a distinct carbonate bed (***a-e***, Figs. 9, 13). These beds are about 20 cm thick and display transitional boundaries with the host sediments, except for bed ***a*** in which the boundaries are sharp. Cycles Pm1-Pm7 have been the object of semiquantitative studies of the calcareous nannofossil and foraminifer assemblages (Lozar et al., 2010; Violanti et al., 2013), of petrographic and geochemical analyses (Dela Pierre et al., 2012), and of paleontological analyses of fish assemblages.

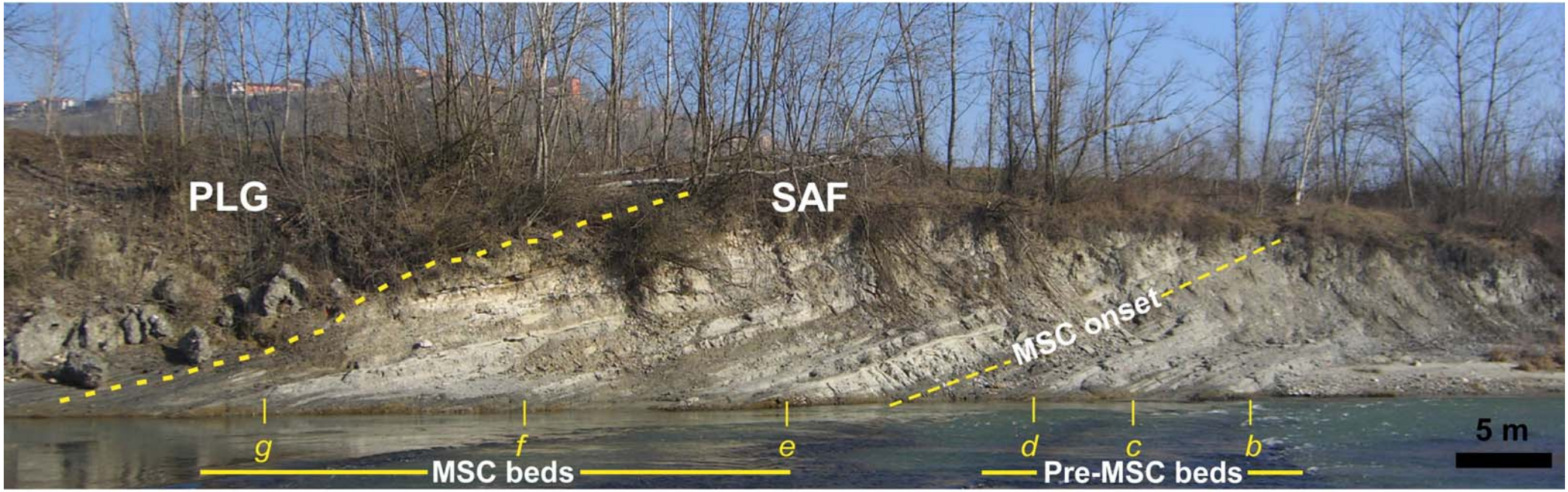

Fig. 13 - Panoramic view of the lower part of the Pollenzo section, showing the boundary between the Sant'Agata Fossili marls **(SAF)** and the primary lower gypsum unit **(PLG)**. The letters indicate the carbonate-rich beds; bed a is not visible from this perspective.

DOI: 10.3301/GFT.2016.03

Micropaleontological and bio-magnetostratigraphic data

Detailed magnetostratigraphic and semiquantitative micropaleontological analyses (calcareous nannofossils and foraminifers) of cycles Pm1-Pm7 have been performed (Fig. 14) (Lozar et al., 2010; Violanti et al., 2013). The interval shows a reversed polarity; unfortunately the base of chron C3r was not identified, probably due to bad preservation of the original magnetic signature. Several bioevents allow the correlation of the Pollenzo section to other reference sections in the PB (Govone) and Mediterranean areas (Fig.15). The peak abundance of *Globigerinoides* spp. and *Globoturborotalita apertura* gr. recognised in cycle Pm1 correlates to cycle Gm25 in the Govone section and to cycle UA31 in the Abad composite section (Sierro et al., 2003).

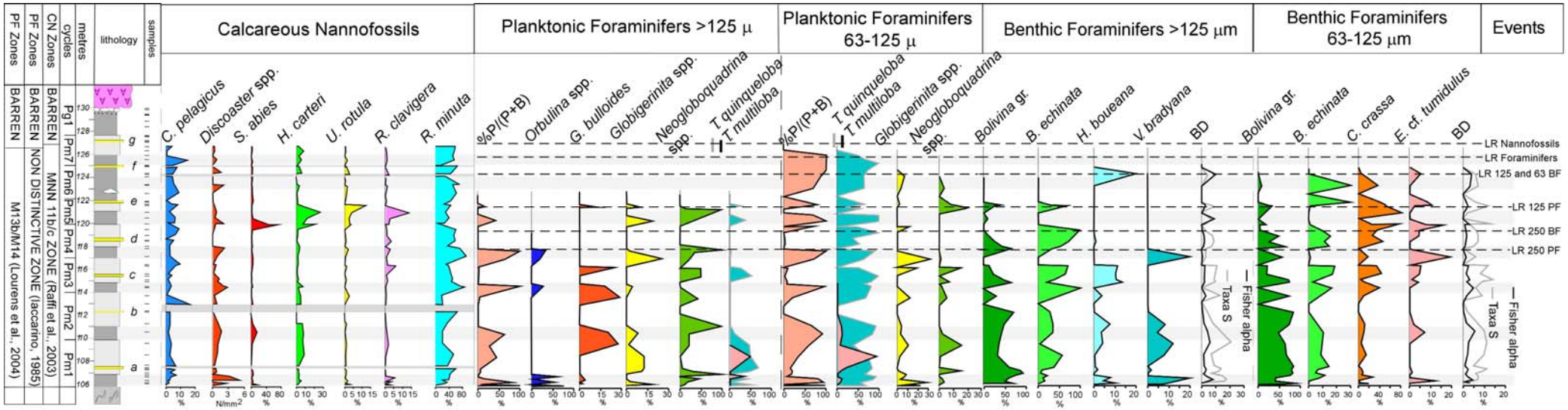

Fig. 14 - Biostratigraphy, lithological column, sample location, percentage variations of the main calcareous nannofossil, planktonic and benthic foraminifer taxa in the Sant'Agata Fossili marls of the Pollenzo section. Dark grey and light grey bands highlight barren intervals and laminated shale intervals, respectively. **BD** = benthic diversity. **LR** = last recovery. (Modified from Violanti et al., 2013). Legend as in Fig. 9.

As in other Mediterranean sections, the lithologic cyclicity reflects climatic changes driven by precessional forcing (e.g. Flores et al., 2005), demonstrated by the fluctuation of warm oligotrophic and temperate/mesotrophic calcareous microfossil assemblages documented in cycles Pm1-Pm4 (opposite abundance peaks of *Discoaster* spp. and *Coccolithus pelagicus* among calcareous nannofossils and *Orbulina*

DOI: 10.3301/GFT.2016.03

universa versus *Neogloboquadrina acostaensis* among foraminifers) (Fig. 14). Laminated shales were deposited during time of seasonal fresh water input, water column stratification, low salinity, oligotrophy or mesotrophy in the upper photic zone and strongly dysoxic bottoms. On the contrary deposition of marls occurred at time of moderate to good mixing in the water column, higher nutrient availability in surface waters and slightly oxygenated sea bottom. Progressively more eutrophic, dysoxic to strongly dysoxic conditions characterised all the succession up to cycle Pm6. At the base of cycle Pm5 the sharp *S. abies* abundance peak occurs and marks the onset of the MSC (Lozar et al., 2010; Dela Pierre et al., 2011). This bioevent, together with higher abundance of stress tolerant taxa among calcareous nannofossils (*Helicosphaera carteri*, *Umbilicosphaera rotula*, *Rhabdosphaera clavigera* and *Reticulofenestra minuta*) and planktonic (*Turborotalita quinqueloba*) as well as benthic foraminifers (*Bolivina* spp., *Bulimina echinata* and *Cassidulina crassa*) records an increasingly stressed paleoenvironment both in the water column and at the sea bottom.
Planktonic foraminifers disappear in the lower half of cycle Pm6, responding to unsuitable water column conditions earlier than calcareous nannofossils, which survive up to cycle Pm7, few metres below the first local gypsum bed.
It is worth noting that the onset of the MSC is located at the base of cycle Pm5 according to micropaleontological data and is marked by the *S. abies* peak; this is in agreement with physical stratigraphic data according to which the SKB (the third local gypsum bed, placed six cycle above the onset) should correspond to the sixth PLG cycle (Dela Pierre et al., 2011). This conclusion allowed us the recognise that in upper part of the Sant'Agata Fossili marls four pre-MSC cycles (Pm1-Pm4) are present, followed by three MSC cycles (Pm5, Pm6, and Pm7) which corresponds to the lower three PLG cycles recognised in the marginal part of the basin.

*Petrographic, geochemical and paleontological data of the **Pre-MSC** cycles*

- *Unconsolidated sediments*

As already stated, the cycles are composed of a basal shaly layer followed by a marly layer (Fig. 9). The total carbonate ranges from 23 to 41% in the homogeneous marl and reaches the lowest values (<23%) in the laminated shale. It consists of both calcite and dolomite, mixed in variable proportion. As a general rule, pre-MSC sediments contain a higher calcite fraction than MSC ones, probably because of the higher content of skeletal grains (foraminifers and calcareous nannofossils), that are generally very rare or even absent in MSC sediments. Articulated fish skeletal remains are rather common in the laminated shales. The fish assemblages of the Sant'Agata Fossili marls primarily consist of epi- and mesopelagic taxa (e.g., Gaudant & Cavallo, 2008), including clupeids (*Alosa elongata*), pearlsides (*Maurolicus muelleri*), deep-sea hatchetfishes (*Argyropelecus*

DOI: 10.3301/GFT.2016.03

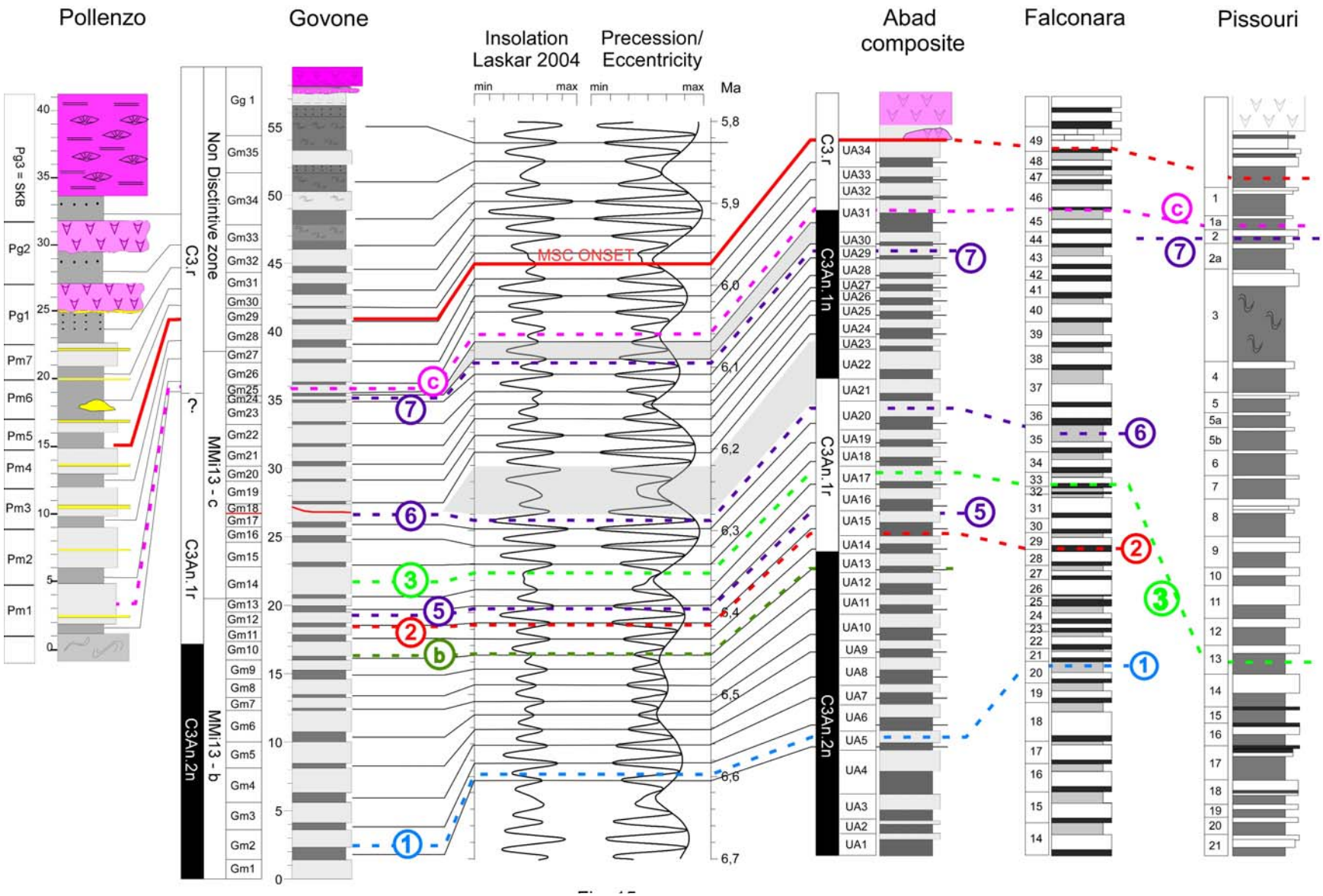

Fig. 15 - Tuning of the Pollenzo (Lozar et al., 2010; Dela Pierre et al., 2011; Violanti et al., 2013) and Govone (Bernardi, 2013) sections with the astronomical solution (65°N summer insolation, precession and eccentricity curves; Laskar et al., 2004) and correlation with other Messinian reference sections from western (Abad composite, Spain; Sierro et al., 2001; 2003)), central (Falconara-Gibliscemi, Sicily – Italy: Hilgen & Krijgsman, 1999; Blanc-Valleron et al., 2002)), and eastern (Pissouri, Cyprus; Krijgsman et al., 2002; Kouwenoven et al., 2006) Mediterranean. Dashed lines and numbers refer to bioevents shown in Fig. 19.

DOI: 10.3301/GFT.2016.03

logearti), lanternfishes (*Lampanyctus* spp.), codlets (*Bregmaceros albyi*), pipefish (*Syngnathus albyi*) and scombrids (*Scomber scombrus*) documenting an open and relatively deep marine basin characterised by (at least) periodic water column stratification.

• *Carbonate beds*

Pre-MSC carbonate beds (Fig. 16A) contain variable amount of a silt-sized terrigenous fraction. They are bioturbated (Fig. 16B), suggesting deposition on an oxygenated sea bottom, and also contain foraminifers and calcareous nannofossils. The intergranular cement consists of idiomorphic rhombohedral dolomite crystals, ranging in size from 2 to 10 μm (Fig. 16C). Calcite is also present, both of biogenic and diagenetic (?) origin. Pyrite framboids are common (Fig. 16D).

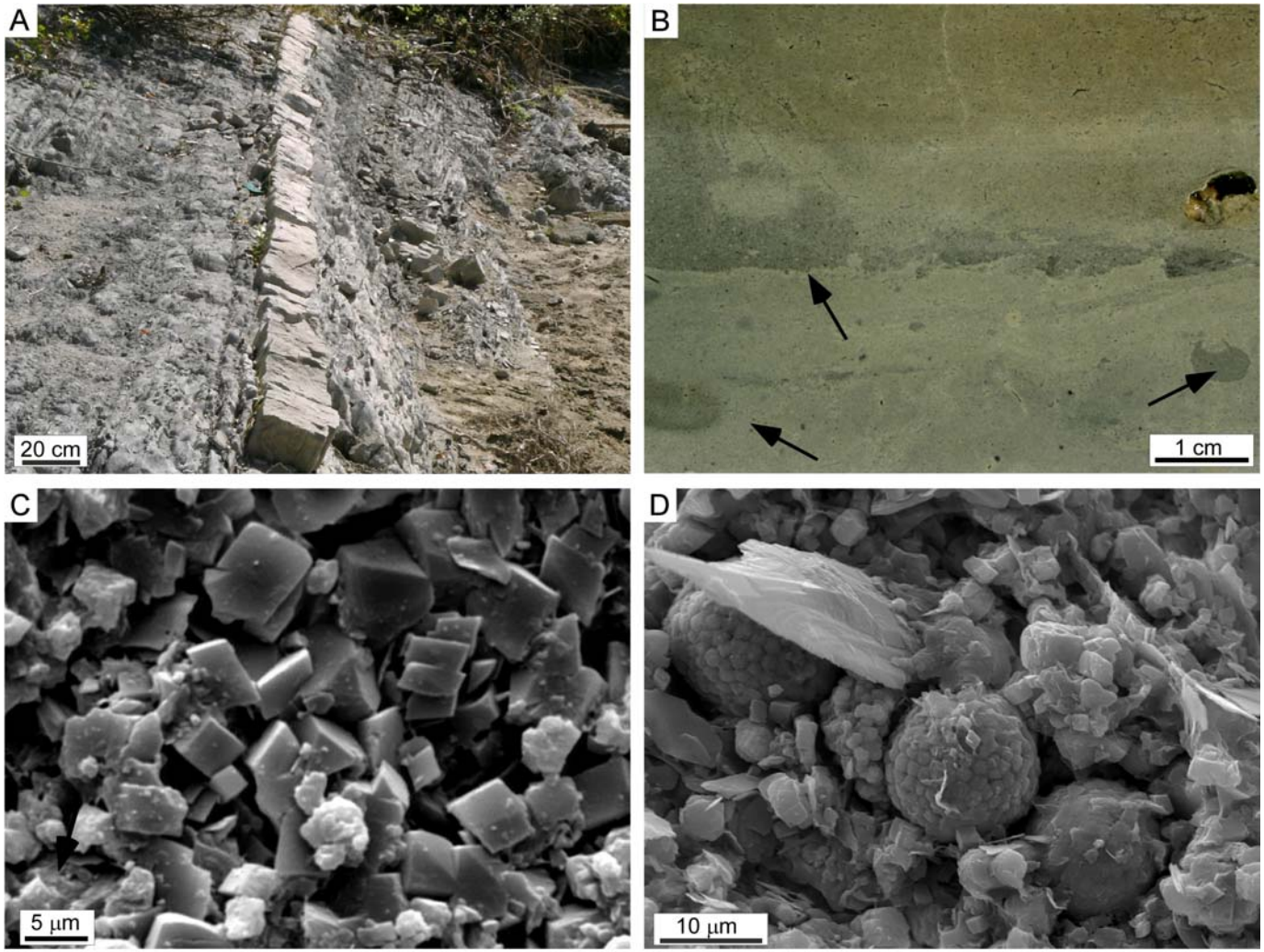

Fig. 16 - Pre-MSC beds. **A)** Outcrop view of bed a. Note the sharp lower and upper boundaries. **B)** Polished slab of bed a. Burrows (arrows) can be recognised. **C)** SEM image of a slightly etched broken chip of bed a. Rhombohedric dolomite crystals are clearly recognisable. **D)** SEM image of a slightly etched broken chip of bed d. Pyrite framboids and dolomite crystals are visible.

DOI: 10.3301/GFT.2016.03

A significant ^{13}C depletion was observed for both dolomite and calcite in beds ***a*** and ***b*** ($\delta^{13}C_{dol}$ = −19.8 and −21‰; $\delta^{13}C_{cal}$ = −16.7 and −14.5‰, respectively) (Fig. 9). In the upper two pre-MSC beds (***c*** and ***d***) less negative values were instead measured for both minerals (−4.4 and −5.2‰ for dolomite; −9.2 and −5.7‰ for calcite, respectively). Positive $\delta^{18}O_{dol}$ values were observed in all pre-MSC beds: the stronger ^{18}O enrichment was measured in beds *a* ($\delta^{18}O_{dol}$ = +7‰) and *b* ($\delta^{18}O_{dol}$ = + 6.9‰), whereas in beds *c* and *d* lower values were found ($\delta^{18}O_{dol}$ = +1.3 and +3.6‰, respectively). More negative values were observed for calcite. In beds ***a*** and ***b*** the $\delta^{18}O_{cal}$ is +5.7 and −1.0‰, respectively, whereas in beds ***c*** and ***d*** it is −3.9 and −1.5‰.

Interpretation

Pre-MSC carbonate beds are composed of predominant dolomite and are interpreted as early diagenetic products formed in the shallow subsurface at the expenses of sediments deposited on an oxygenated sea bottom during precessional insolation minima. The occurrence of authigenic dolomite and pyrite and the negative $\delta^{13}C$ values measured in diagenetic dolomite of the lower two beds (***a*** and ***b***) ($\delta^{13}C$ around −20‰), points to the contribution of anaerobic oxidation of methane in dolomite precipitation. The moderate ^{13}C depletion (compared to typical methane-derived carbonates in which $\delta^{13}C$ values as low as −60‰ are commonly measured; *e.g.* Peckmann & Thiel, 2004) may reflect the mixture of methane-derived carbon with other sources, such as heavier hydrocarbons (Roberts & Aharon, 1994), marine dissolved inorganic carbon or skeletal material of marine organisms, which are actually present in these beds (*e.g.* Natalicchio et al., 2012). Conversely, the less negative $\delta^{13}C$ values of beds ***c*** and ***d*** ($\delta^{13}C$ around −5‰) suggest that dolomite precipitation was induced by organoclastic bacterial sulphate reduction alone, as the upward methane flux ceased completely. Sulphate reduction alone, however, was able to produce only a lesser amount of authigenic dolomite with respect to anaerobic oxidation of methane, as indicated by the minor induration of these beds. The oxygen isotope record of dolomite (the predominant carbonate mineral) reveals that beds ***a*** and ***b*** are significantly enriched in the heavy ^{18}O isotope. The explanation of such an enrichment is problematic: it could reflect the involvement of evaporated waters (*e.g.* McKenzie et al., 1979*;* Bellanca et al., 2001; Blanc-Valleron et al., 2002) or deep diagenetic fluids, possibly sourced from gas hydrate destabilisation (e.g. Aloisi et al., 2000) The first mechanism is difficult to accept, because these beds formed before the onset of the MSC; moreover it strongly contrasts with the negative $\delta^{18}O$ values of the host sediments (up to −5 ‰). The possible involvement of gas hydrate destabilisation is consistent with the association of positive $\delta^{18}O$ values with negative $\delta^{13}C$ ones. This mechanism has already been suggested for lower Messinian dolomite layers and concretions found in the eastern part of the Piedmont basin (Dela Pierre

DOI: 10.3301/GFT.2016.03

et al., 2010; Natalicchio et al., 2012; 2013), Spain and Northern Morocco (Pierre & Rouchy, 2004). The lower oxygen values measured in beds ***c*** and ***d***, that are coupled with slightly negative $\delta^{13}C$ ones, suggest that the input of ^{18}O-enriched fluids ceased, together with the demise of methane-rich fluids.

*Petrographic, geochemical and paleontological data of the **MSC** cycles*

• *Unconsolidated sediments*

MSC cycles (Fig. 17A) show analogous lithologic characteristics of pre-MSC ones, but no marls were observed in cycle PM6. These unconsolidated sediments display a similar composition of the carbonate fraction, but the calcite content is lower, due to the scarcity or absence of skeletal grains (foraminifers and calcareous nannofossils).

The laminated shales of the MSC cycles contain fossil fish remains represented by abundant well-preserved articulated skeletons of the Palaeomediterranean Messinian cyprinodontid *Aphanius crassicaudus* and, very rarely, by gobies or sea breams. The hypoxic-anoxic conditions that persisted in the lower part of the water column leading to the deposition of the shales of the MSC cycles resulted in the preservation of part of the original pigmentation of the scales, abdominal cavity and median fins in several specimens of *Aphanius crassicaudus*. Some specimens exhibit vertical black stripes running the depth of the caudal fin plus a nearly horizontal black stripe that run the dorsal-fin base. In extant fishes, the black coloration derives from the dispersion of melanin in the melanophores. Scattered small black dots are also present on body scales and possibly represent preserved invidual melanophores, and the black stripes in the caudal and dorsal fins might be composed by the chemical residues of the original melanin pigments.

• *Carbonate beds*

Beds deposited during the salinity crisis display different characteristics. Bed ***e*** is located at the top of the marly interval and contains mm-sized intraclasts, floating in a clotted micrite matrix containing rare foraminifers. A remarkable feature is the presence of contractional cracks developed around the clasts (circumgranular cracks). Bed ***f*** lies in strongly laminated shales (Fig. 17B) and shows a lamination marked by the alternation of mm-thick whitish and grey wrinkled laminae (Fig. 17C). Whitish laminae are composed of clotted micrite and contain abundant pyrite framboids. These laminae exhibit a strong epifluorescence, suggesting a higher content in organic matter, contain abundant fish vertebrae and scales and filamentous fossils, up to 100 μm across and more than 300 μm long, showing different fluorescence shades (Fig. 17F). The grey laminae are richer in terrigenous material, mostly represented by clay particles and mica flakes.

DOI: 10.3301/GFT.2016.03

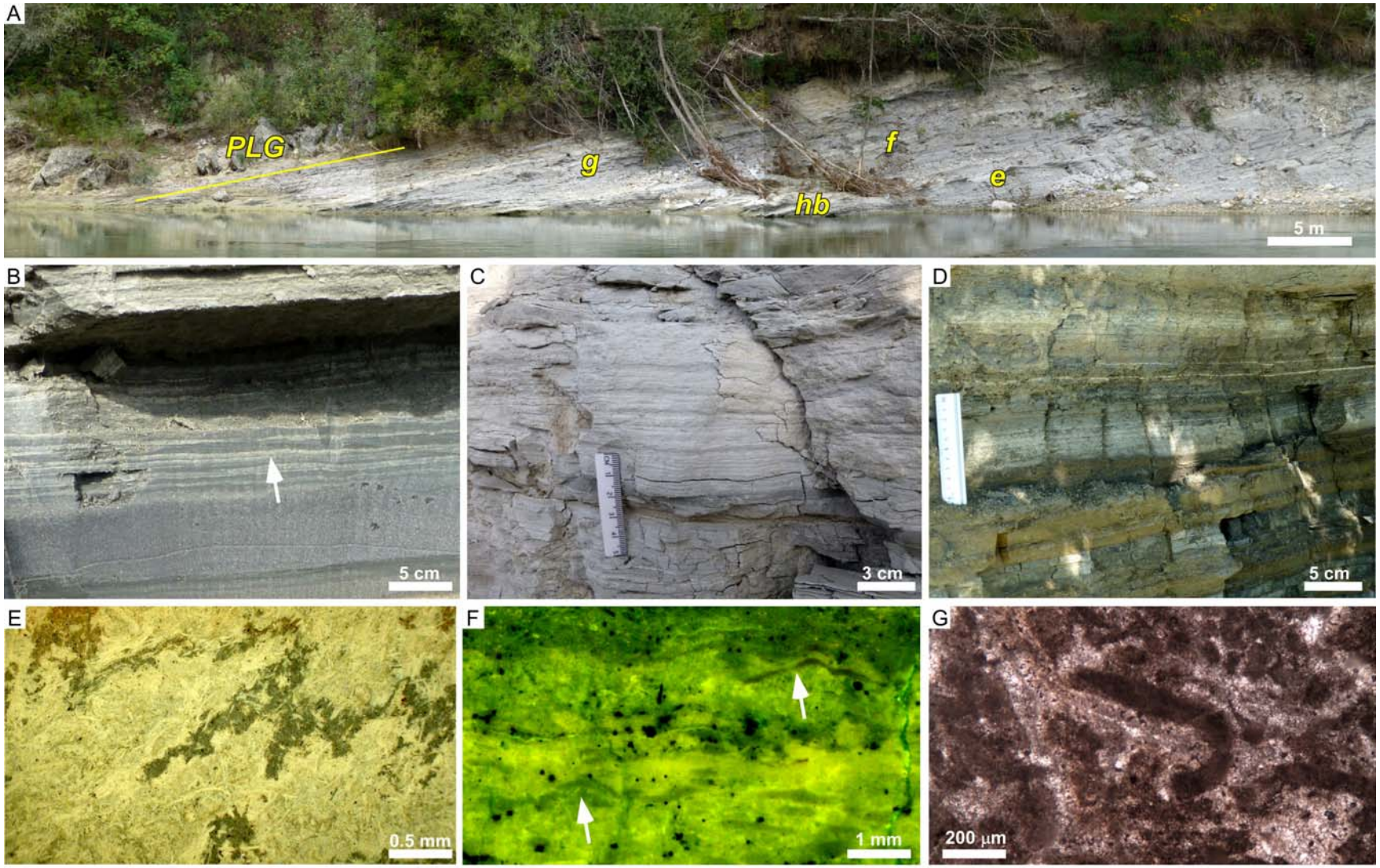

Fig. 17 - MSC beds. **A)** Outcrop view of the uppermost part of the Sant'Agata Fossili marls. Beds e, f and g, the hemi-ellipsoidal body (hb) and the first PLG layer can be recognised. **B)** The laminated shales below bed f; mm-thick whitish laminae can be recognised (arrow). In these laminae, filamentous fossils were observed (cf. Fig. 17E). **C)** Outcrop view of bed f; the laminated structure, given by whitish carbonate laminae and grey terrigenous ones is recognisable. **D)** The shaly interval below the first gypsum layer (cycle Pg1): thin sandy layers are interbedded with grey shales and laminated whitish layers containing filamentous fossils. **E)** Polished slab, cut parallel to the bedding of a whitish lamina below bed f (cf. Fig. 17B). A maze of whitish filaments can be recognised. **F)** Photomicrograph in epifluorescence of bed f. Note the stronger fluorescence of a carbonate lamina. Filaments (arrows) can be seen. **G)** Photomicrograph (plane light) of a curved filament from the hemi-ellipsoidal body.

DOI: 10.3301/GFT.2016.03

Filamentous fossils were recognised in the unconsolidated shales, below and above the cemented layer, within mm-thick whitish laminae (Fig. 17E). Bed ***g*** is similar to bed ***f***, except for the more wrinkled and thinner laminae (less than 1 mm). Pyrite framboids are abundant and are frequently grouped together to mimic filaments about 100 μm across and up to 800 μm long. Whitish filaments were also observed in the shaly part of cycle PLG 1, immediately below the first gypsum bed (Fig. 17D). Remarkably, no terrigenous grains, abundant in the enclosing matrix, were observed within the filaments of beds ***e*** and ***g***.
Unlike the pre-MSC beds, the carbonate fraction of the MSC layers is dominated by calcite whereas dolomite is subordinate (Fig. 9).
Filamentous fossils were also observed in a metre-sized hemi-ellipsoidal cemented body within cycle Pm6 (Fig. 17G). The filaments are made of clotted micrite, composed of micron-sized strongly epifluorescent calcite crystals. They are commonly curved and are surrounded by fringing aragonite. Pyrite framboids, up to 20 μm across, are very common in both types of laminae and frequently cap acicular aragonite crystals.
In the salinity crisis beds, the $\delta^{13}C$ values of both dolomite and calcite are moderately negative (from –5 to –3.9‰ for dolomite and from –7.9 to –6.7‰ for calcite) (Fig. 9). A stronger ^{13}C depletion was measured for the calcite of the hemi-ellipsoidal body (cycle Pm6), with values around –8.5‰. For what concerns the $\delta^{18}O$, a remarkable shift towards negative values was observed. The $\delta^{18}O_{dol}$ values range from –6.1 to –4.9‰ whereas the $\delta^{18}O_{cal}$ are more negative (from –6.5 to –8.8‰). The hemiellipsoidal body yielded $\delta^{18}O_{cal}$ values as low as –7.7‰ (Fig. 9).

Interpretation

A sharp change of sedimentological, compositional and geochemical characteristics is observed in the MSC beds (Dela Pierre et al., 2012). This change is shown by the following features:
a) the presence of wrinkled laminae containing filament remains; b) the sharp decrease of dolomite and the concomitant increase of calcite (and aragonite); c) *the negative* $\delta^{18}O$ *values of the MSC carbonates.*

a) Microbial filaments are common in Messinian gypsum crystals (the so called *spaghetti*-like structures; Vai & Ricci Lucchi, 1977) and interpreted as remains of photosynthetic cyanobacteria (*e.g. Scytonema*) (Rouchy & Monty, 1981; Panieri et al., 2010). Analogous features were observed in Messinian carbonate deposits below the gypsum and were considered either as fecal pellets (Guido et al., 2007) or as cyanobacteria remains on the basis of their similarities with the *spaghetti* structures (Rouchy & Monty, 1981; Orszag-Sperber et al., 2009). The

DOI: 10.3301/GFT.2016.03

absence of terrigenous grains within the Pollenzo filaments allows us to rule out their fecal origin. An alternative hypothesis is that these filaments represent remains of colourless sulphide-oxidizing bacteria like *Beggiatoa* and *Thioploca* (Oliveri et al., 2010). These giant bacteria obtain the energy necessary for their life from the oxidation of sulphide by using oxygen or nitrate as electron acceptors (Schulz & Jørgensen, 2001) and do not require light as the driving energy source. In modern settings, they form dense microbial mats thriving at different water depth (from peritidal to bathyal settings), at sites where high concentration of sulphide is available at the sea bottom (*e.g.* Bailey et al., 2009) such as hydrothermal vents (*e.g*. Jannasch et al., 1989), cold seeps (Sahling et al., 2002; Teichert et al. 2005) or where organic-rich sediments are exposed at the sea floor in contact with either oxic (Schulz et al., 1999) or oxygen-depleted waters (Gallardo, 1977). In the last case the bacteria use nitrate (and not oxygen) as electron acceptor for oxidizing sulphide to sulphate.

Although there are substantial similarities between the filamentous cyanobacteria and the sulphide-oxidizing bacteria and their distinction is difficult on morphology only, we have proposed that the Pollenzo filaments are remains of sulphide-oxidizing bacteria (Dela Pierre et al., 2012) on the basis of the following elements: 1) their diameter (>100 μm), that is close to that of living forms; on the contrary, cyanobacteria filaments rarely exceed 80 μm (*e.g*. Schulz & Jørgensen, 2001); 2) the curved shape of some filaments (Fig. 17G) consistent with the chemotactic behaviour of these prokaryotes that often change their direction in the search of optimal concentrations of oxygen or nitrate (*e.g.* Møeller et al., 1985; Oliveri et al., 2010); 3) the concentration of iron sulphide grains outlining the filament shape (beds *f* and *g*); living sulphide-oxidizing bacteria host elemental sulphur globules within the cytoplasm, that can be further preserved as sulphur-containing minerals associated to the filamentous body fossil (*e.g.* Bailey et al., 2009); 4) the lack of any remain of shallow water macrobiota that should accompany photosynthetic mats. The only features that could suggest a shallow water origin for these laminated layers are the contractional cracks, previously interpreted as desiccation structures and hence considered as a compelling evidence of the subaerial exposure of the Piedmont basin at the onset of the MSC (Sturani, 1973). These features can alternatively be interpreted as the product of syneresis, related to the decay of bacterial extracellular polysaccharide substances (EPS) binding clay particles (*e.g.* Hendry et al., 2006) in a subaqueous environment. On this basis, beds *f* and *g* and the hemi-ellipsoidal body of cycle Pm6 are interpreted as the product of the lithification of chemotrophic microbial mats dominated by sulphide-oxidizing bacteria. Their growth was triggered by the establishment of dysoxic to anoxic conditions at the sea bottom (hampering gypsum deposition; e.g. De Lange & Krijgsman, 2010), in turn related to density

DOI: 10.3301/GFT.2016.03

stratification of the water column and/or enhanced primary productivity in the water column. Preservation of the delicate filamentous structure was due to precipitation of a substantial carbonate fraction (mostly calcite). The slightly depleted $\delta^{13}C$ values points to degradation of organic matter via bacterial sulphate reduction as the triggering mechanism. This process provided the hydrogen sulphide fluxes necessary for the sustainment of chemotrophic mats at the sea bottom. However, it was argued that sulphide oxidation, that promotes acidity and carbonate dissolution, was temporarily and spatially decoupled from the alkalinity generated by sulphate reduction and inducing carbonate precipitation, since this process occurred within already buried mats, where the preferential sites for carbonate formation were dead bacterial filaments in which more reactive organic matter was available (Dela Pierre et al., 2012; 2014).

b) Although still discussed (Sánchez-Román et al., 2009), the concentration of sulphate in the pore waters is a critical factor controlling the composition of bacterially-induced carbonate minerals. In particular, if the concentration of sulphate is high, dolomite is inhibited and other carbonates (aragonite, calcite, Mg-calcite) do form (*e.g.* Baker & Kastner, 1981; Kastner, 1984; Wright & Oren, 2005). It is proposed that in pre-MSC beds the sulphate in pore waters was exclusively supplied by normal salinity sea water and carbonate precipitation took place within the sedimentary column. Under these conditions, all sulphate was consumed by bacterial sulphate reduction and dolomite precipitation took place from sulphate-free pore waters (Dela Pierre et al., 2012).On the contrary, MSC carbonate beds deposited at the sea bottom in contact with sulphate-enriched bottom waters, being these layers the lateral equivalents of bottom-grown selenite beds formed in the shallower part of the basin, some tens of kilometres apart. Moreover, the sulphate pool was continuously replenished by sulphide oxidation in the chemotrophic microbial mats. As a consequence, sulphate could not be totally consumed, even in the presence of an intense bacterial sulphate reduction, and precipitation of Ca-carbonates was favoured. Minor amounts of dolomite formed after sediment burial, when all sulphate was consumed.

c) The shift towards more negative $\delta^{18}O$ values observed in MSC carbonates ($-6.5 < \delta^{18}O_{cal} < -8.8$‰ PDB; $-4.9 < \delta^{18}O_{dol} < -6.1$‰ PDB) compared to the underlying pre-MSC ones remains a still unresolved question. Such ^{18}O depletion is reported from carbonates just below the first evaporitic deposits in other Mediterranean basins (even if less severe than at Pollenzo) and is interpreted as the result of sharp dilution events pointing to the isolation of the basin(s) prior to the onset of gypsum deposition (*e.g.* Bellanca et al., 2001; Blanc-Valleron et al., 2002). Alternative hypothesis have been proposed, suggesting microbial sulphate consumption as a possible source of ^{16}O enrichment in the microenvironments of carbonate precipitation (Sass et al., 1991; Brunner et al., 2005; Wortmann et al., 2007).

DOI: 10.3301/GFT.2016.03

Stop 1C - Slumped and chaotic deposits (second stage of the MSC)

In this stop we will observe a slumped interval interbedded between the PLG unit and the Cassano Spinola conglomerates (Fig. 9). This interval is considered as the lateral equivalent of the Valle Versa chaotic complex (exposed in the Monferrato sector), deposited during the second MSC stage (Dela Pierre et al., 2011). It is about 5 m thick and consists of extensively deformed organic-rich shales (Fig. 18A). These enclose a m-sized gypsum block with the same characteristics of the layers composing the upper PLG cycles. Irregularly-shaped carbonate concretions and cm-thick carbonate layers are also present. The slumped interval is followed by about 2 m of shales crossed by carbonate cemented clastic dykes. Articulated skeletons of the cyprinodontid *Aphanius crassicaudus* are relatively common in the shales overlying the slumped interval.

Stop 1D - The Cassano Spinola conglomerates

This unit, deposited during the third stage of the MSC (Dela Pierre et al., 2011), can be split in two sub-units.

Sub-unit a

Sub-unit a consists of grey muds and yellowish silty muds that are locally very rich in land plant debris and leaves. The presence of *in situ* root traces and mud cracks suggest conditions of subaerial exposure. These fine-grained sediments are interpreted as alluvial plain, overbank or waning flood deposits (Colombero et al., 2014). Three/four lens-shaped conglomeratic layers, some of which with spectacular cross bedding (Fig. 18B) are interbedded to the fine-grained deposits. The conglomeratic layers are composed of rounded and smoothed selenite clasts as well as of pebbles of Alpine metamorphic rocks and are interpreted as fluvial deposits. A rich and diversified vertebrate fauna has been found in this sub-unit, indicating that at the end of the Messinian, the Piedmont region was an important cross-road for faunal dispersal in the emerging Italian peninsula (Colombero et al., 2014). Amphibians and reptiles including testudinid and geoemydid turtles, lacertids, an agamid, a varanid, a small snake of the infraorder Scolecophidia and a colubrid, are some elements of the rich and diverse herpetofaunal fossil assemblages. Bird remains are scarce and consist of a phasianid and two birds of prey, an acipitrid and a strigid. Large sized herbivores such as a gomphotheriid, a rhinocerotid, giraffids, a camelid, together with an hipparionin horse, cervids, bovids, antilopines of the genus *Gazella*, and carnivores like the small canid *Eucyon*, the large sized saber-toothed cat *Amphimachairodus giganteus* and the cursorial hyaenid *Hyaenictitherium* are the most common large mammals (Colombero et al.,

DOI: 10.3301/GFT.2016.03

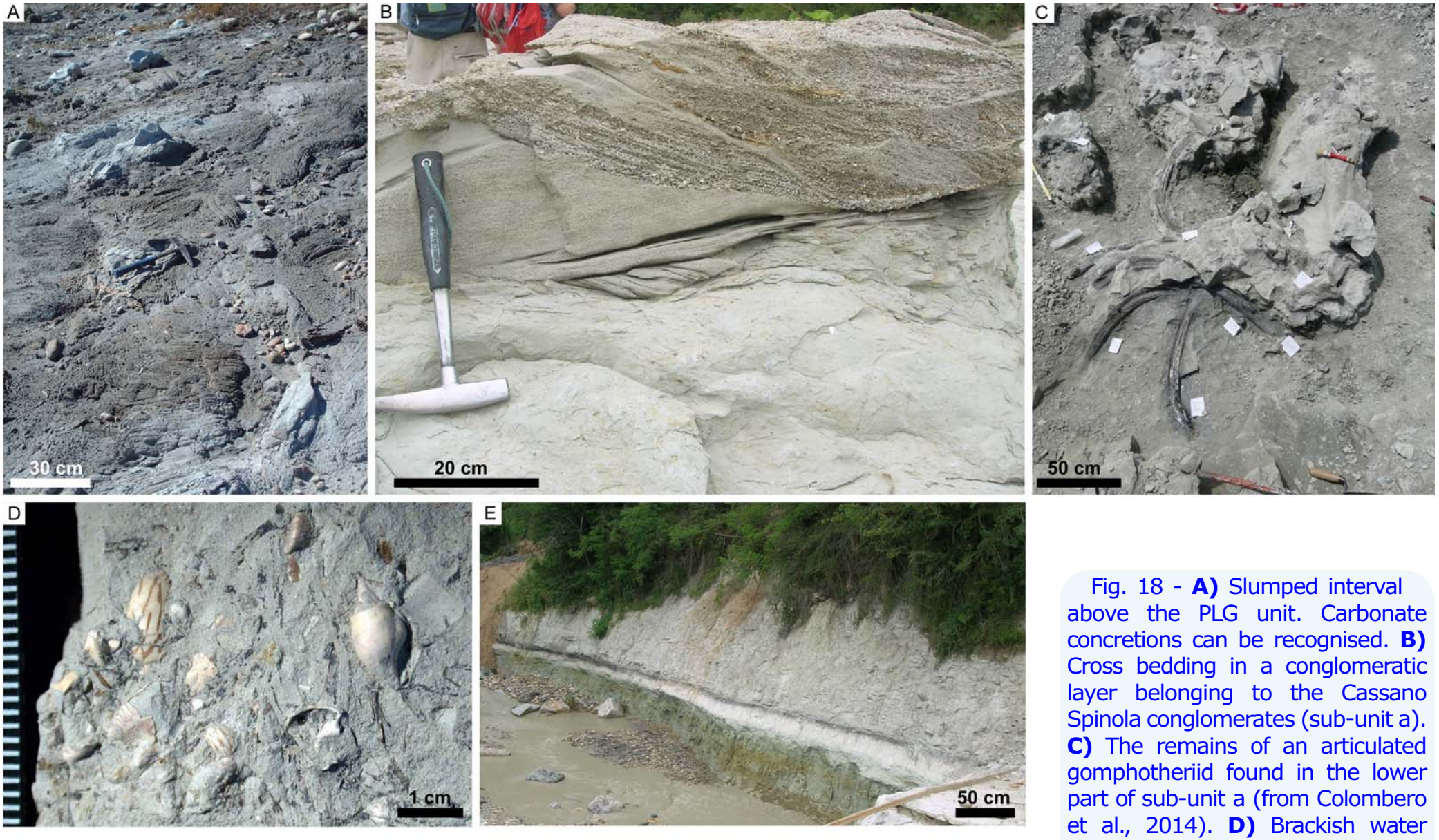

Fig. 18 - **A)** Slumped interval above the PLG unit. Carbonate concretions can be recognised. **B)** Cross bedding in a conglomeratic layer belonging to the Cassano Spinola conglomerates (sub-unit a). **C)** The remains of an articulated gomphotheriid found in the lower part of sub-unit a (from Colombero et al., 2014). **D)** Brackish water molluscs (*Congeria* and *Melanopsis*) from sub-unit b (photo courtesy of E. Martinetto). **E)** the Messinian-Zanclean boundary, marked by a characteristic black layer.

2014). The presence of articulated skeletal remains of large mammals, such as those referred to a single individual of a gomphotheriid (Fig. 18C), a large proboscidean, testify the limited or absent degree of reworking that affected the vertebrate remains found in the finest sediments. Small mammals are quite

DOI: 10.3301/GFT.2016.03

abundant and represented by insectivores and rodents among which murids are the most common elements (Colombero et al., 2013). Overall, the vertebrate assemblages recovered from the sub-unit a testifies the presence of open habitats close to woodlands, the latter probably related to the presence of fresh and brackish water bodies. Disarticulated fish bones belonging to *Aphanius crassicaudus,* charophyte gyrogonites and ostracods occur in some layers, suggesting the presence of water bodies characterised by broad salinity excursion. The occurrence of a single otolith belonging to what appears to be a lophiiform fish, a stenohaline marine taxon, in these deposits is intriguing, suggesting that a basin filled with marine waters was present not far from continental setting documented by the Cassano Spinola conglomerates.

Sub-unit b

This sub-unit (Strati a Congeria *sensu* Sturani, 1973) is made up of grey marls that contain, especially in the middle and topmost part, brackish water fossil assemblages of the "Lago Mare" biofacies (Fig. 18D). These consist of molluscs (*Dreissena*, *Melanopsis*, limnocardiids) and ostracods (*Amnycithere propinqua*, *Cyprideis agrigentina*, *Loxoconcha muelleri*) that allow correlation with the *Loxoconcha muelleri* Biozone (Grossi *et al.* 2011), thereby suggesting an age probably not younger than 5.40 Ma. In the lower part a characteristic black silty layer, very rich of land plant debris, was observed and interpreted as a marsh deposit. The top of sub-unit b (now submerged by the Tanaro river) is intensively burrowed: a network of firm grounds burrows, filled with a black silty mud that marks the boundary between the Messinian and the Zanclean could be observed.

The Messinian/Zanclean boundary

The boundary between the Messinian Cassano Spinola conglomerates (sub-unit b) and the Zanclean Argille Azzurre Fm. was sampled two years ago. Now the outcrop is submerged by the Tanaro river and is no longer accessible. The boundary is marked by a 30-40 cm thick black muddy layer (Fig. 18E). This layer is intensively burrowed by large firm ground burrows filled with the overlying sediments of the Argille Azzurre Fm. This ichnological association confirms a sharp decrease of the net sedimentation rate and starved conditions at the onset of the Zanclean marine reflooding.

The Argille Azzurre Fm. consists of massive grey calcareous marl, that contain, from the base, foraminifers and calcareous nannofossils. Preliminary analyses of calcareous nannofossils assemblage of the lower five metres of the Argille Azzurre Fm. have shown the continuous occurrence of *Reticulofenestra cisnerosii*, index species of the lowermost Zanclean calcareous nannofossil MNN12a subzone (Di Stefano & Sturiale, 2010). Moreover,

DOI: 10.3301/GFT.2016.03

semiquantitative analyses have shown a cyclic oscillation of the relative abundance of *Discoaster* spp., that are ascribed to precessional index variation modulating global insolation trends, as already demonstrated for Pliocene sediments (Gibbs et al., 2004). These cycles are only recorded by micropaleontological content fluctuations, but lack lithological evidence. Planktonic foraminifer assemblages show the two peaks of *Neogloboquadrina acostaensis* sinistral recorded in the Mediterranean lowermost Pliocene (Di Stefano et al., 1996). These data suggest that the record is complete and no hiatus occurs at the base of the Pliocene. This is also confirmed by preliminary magnetostratigraphic data (Bernardi & Zanella, pers. com.), documenting the base of Chron C3r.4n three cycles above the base of the Argille Azzurre Fm. Moreover, the occurrence of *Sphaeroidinellopsis* spp., a deep mesopelagic taxon that required a water column at least 600-800 m deep (Kennett & Srinivasan, 1993), confirms an open marine epibathyal paleoenvironment in the Pollenzo area during the lowermost Zanclean, as previously documented in the Torino Hill (Violanti et al., 2011).

STOP 2 - The Govone section

Also this section is located on the banks of the Tanaro river and comprises the whole Messinian succession *i.e.* the Sant'Agata Fossili marls, the PLG unit, the lateral equivalent of the Valle Versa chaotic complex, and the lower part of the Cassano Spinola conglomerates (Fig. 19). The facies however, are significantly different from those observed at Pollenzo, because of the more distal position of this section (close to the Savigliano basin depocentre).

Sant'Agata Fossili marls

A total of 35 lithologic cycles (Gm 31-35, Fig. 19) , each about 3 m thick and composed of shale/marl couplets, are exposed in Govone. In the topmost part (cycles Gm33-Gm35), bedding is deformed by slumping, making the recognition of the lithological cyclicity complex (Fig. 19).

Micropaleontological and biomagnetostratigraphic data

The abundance fluctuations of foraminifer and calcareous nannofossil assemblages in the two lithology (warm water oligotrophic taxa and absent or very scarce stress tolerant benthic taxa in the shaly beds; cooler water eutrophic taxa in the marls) suggest that the lithologic cycles are driven by astronomical (precessional) forcing (Bernardi, 2013). Bed by bed straightforward correlation to other reference sections of the Mediterranean area (Abad

DOI: 10.3301/GFT.2016.03

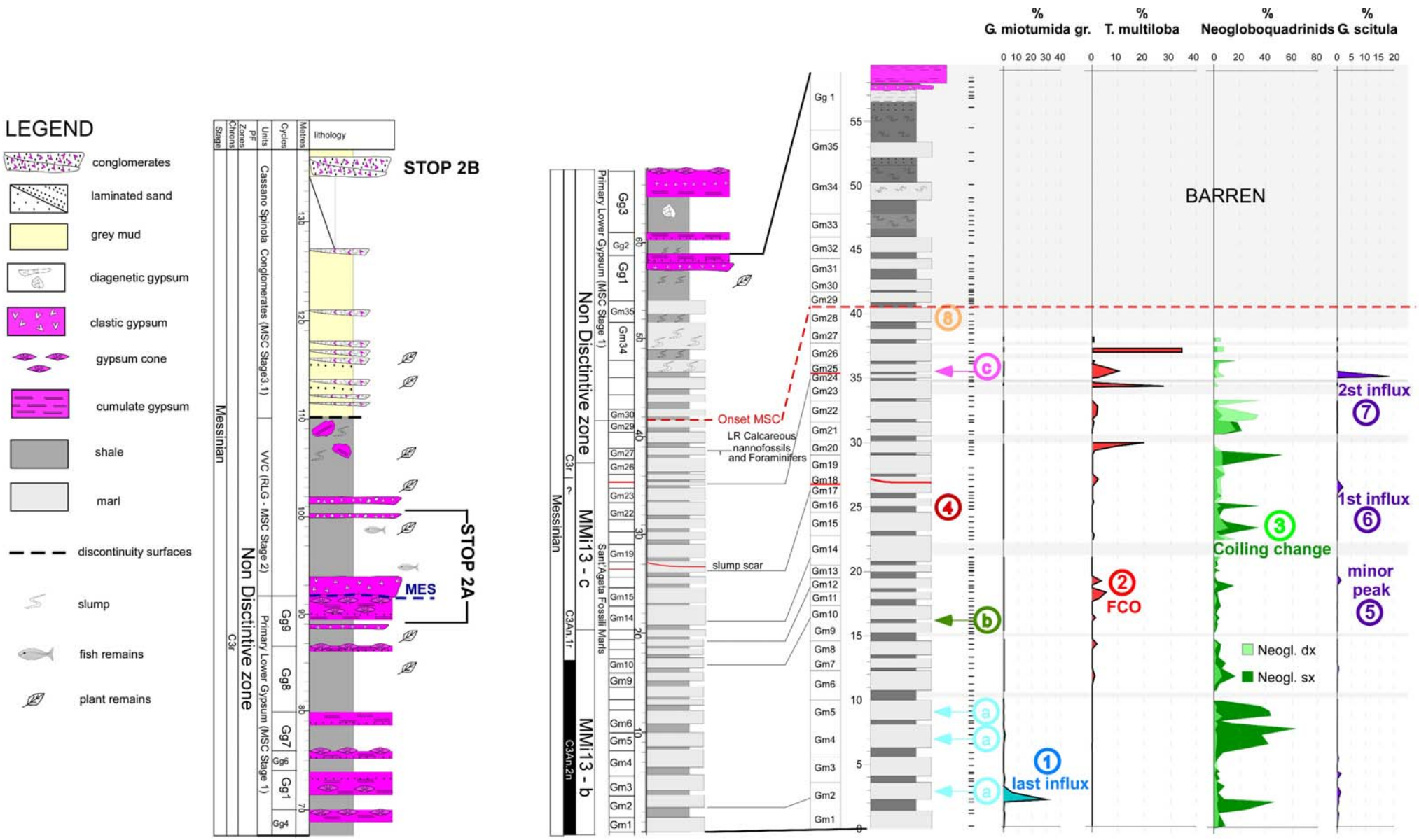

Fig. 19 - The Govone section and main biostratigraphic events recognised in the upper part of the Sant'Agata Fossili marls. Dashed lines and numbers refer to the following bioevents: **1)** Last influx of *G. miotumida* group; **2)** First common occurrence (FCO) of *T. multiloba*; **3)** left/right (S/D) coiling change of *N. acostaensis*; **4)** First occurrence (FO) of *B. echinata*; **5)**, **6)**, **7)** Influxes of *G. scitula*; **8)** Last occurrence (LO) of foraminifers and calcareous nannofossils; a) Influxes of *N. atlantica*; b) disappearance of warm water oligotrophic forms (*Orbulina* spp.); c) Peak abundance of *Globigerinoides* spp. and *Globoturborotalita apertura* gr. Biostratigraphic data from Bernardi (2013).

DOI: 10.3301/GFT.2016.03

composite, Falconara and Pissouri; Sierro et al., 2001; 2003; Hilgen & Krijgsman, 1999; Blanc-Valleron et al., 2002; Krijgsman et al., 2002; Kouwenoven et al., 2006) is based on detailed biomagnetostratigraphic data and the recognition of several planktonic foraminifer bioevents and magnetic reversals. Most important are (Fig.19): 1) the base of the C3An.1r chron in cycle Gm11 (dated at 6.44 Ma); 2) the *Globorotalia scitula* 2nd influx in cycle Gm24 (correlated to cycle UA29 in the Abad section and dated at 6.1 Ma); 3) the *Globigerinoides* spp. and *G. apertura* gr. abundance peaks just above it (cycle Gm25, correlated to UA31 in the Abad composite).
In this section the integration of biomagnetostratigraphic data and recognition of lithologic cycles allows to place the onset of the MSC, i.e. the time line 5.97 (Manzi et al., 2013), at cycle Gm 29 (Fig. 20A), seven cycles below the first local gypsum bed (Gg1, Figs. 15, 19). The last recovery of calcareous microfossils occurs in cycle Gm27, *i.e*. two cycles below the MSC onset (Bernardi, 2013). This prevents the recovery of the *S. abies* peak, that in other PB sections marks the MSC onset (see Pollenzo section; Lozar et al., 2010; Violanti et al., 2013). Hence, the last occurrence of foraminifer and calcareous nannofossils is diachronous over a lateral distance of few kilometres (see Pollenzo section) and cannot be used to approximate the onset of the MSC.

Stop 2A - PLG unit and RLG unit

In this stop, the upper gypsum layer of the PLG unit (GG9) can be observed, and in particular the laminated facies (Fig. 8C) and conical structures ("*padellini*") growing within it (Figs. 20B, D, E). The primary gypsum is sharply overlaid by a layer of clastic gypsum (Fig. 20C), showing normal grading and composed of clasts of twinned-selenite crystals (Figs. 20F, G). This layer introduces the RLG unit and its lower boundary has been correlated to the Messinian erosional surface. Two additional layers of clastic gypsum, interbedded with laminated shales with remains of land plant remains and articulated skeletons of the euryhaline cyprinodontid fish *Aphanius crassicaudus*, can be observed in the upper portion. The RLG unit, that is in this section about 20 m thick, terminates with a slumped interval in which bedding is extensively deformed.

Stop 2B - The Cassano Spinola conglomerates

The slumped interval at the top of the RLG is sharply overlaid by the Cassano Spinola conglomerates. At the base of this unit, thin layers of laminated sands and lenticular shaped conglomeratic beds are interbedded with grey shales. The conglomerates are composed of rounded and smoothed gypsum clasts (in contrast to the twinned selenite clasts found in the RLG units) and of pebbles of Alpine metamorphic rocks that were not observed in the underlying unit. A conglomerate layer with cross stratification can be observed at the top of the section (Fig. 20H).

DOI: 10.3301/GFT.2016.03

Fig. 20 - **A)** The onset of the MSC at Govone (cycle Gm29). **B)** The boundary between the PLG unit and the RLG unit (Valle Versa chaotic complex). The arrows indicate the flattened cones within the laminated gypsiferous silty mudstones. MES: Messinian erosional surface. **C)** Detail of B), showing a layer of clastic gypsum above the primary gypsum (cycle Gg9). **D)** Detail of B, showing flattened cones ("padellini") growing within the gypsiferous silty mudstones. **E)** Detail of a flattened cone. **F)** The graded layer of clastic gypsum above the MES. **G)** Detail of F, showing clasts of selenite crystals. **H)** Cross bedding in a conglomeratic layer (Cassano Spinola conglomerates).

DOI: 10.3301/GFT.2016.03

Day 2 - The northern margin of the Piedmont basin

The northern margin of the Piedmont basin (Monferrato/Torino Hill arc)

In the northern margin of the PB, the MSC deposits are exposed on the southern side of the Monferrato-Torino Hill arc, interbedded between the Tortonian-Lower Messinian Sant'Agata Fossili marls (or older deposits) and the Zanclean Argille Azzurre Fm. Outcrops are in general of very bad quality and the only exposures are located in active gypsum quarries. As stated above, the deposition of the Cenozoic sediments of the Monferrato was strongly controlled by tectonic activity along long-lived NW–SE transpressive faults (Rio Freddo and Villadeati faults) that was responsible for the articulation of the basin in more subsiding areas and intervening structural highs (Clari et al., 1995; Piana, 2000; Dela Pierre et al., 2003). The lateral distribution of the Messinian sediments suggests that these faults were active during the MSC. Two main Messinian sub-basins have been distinguished (Fig. 21): the Moncalvo (to the E) and the Murisengo (to the W) sub-basins which are separated by the Villadeati fault. The Murisengo sub-basin is in turn separated from the Torino Hill by the Rio Freddo fault zone.

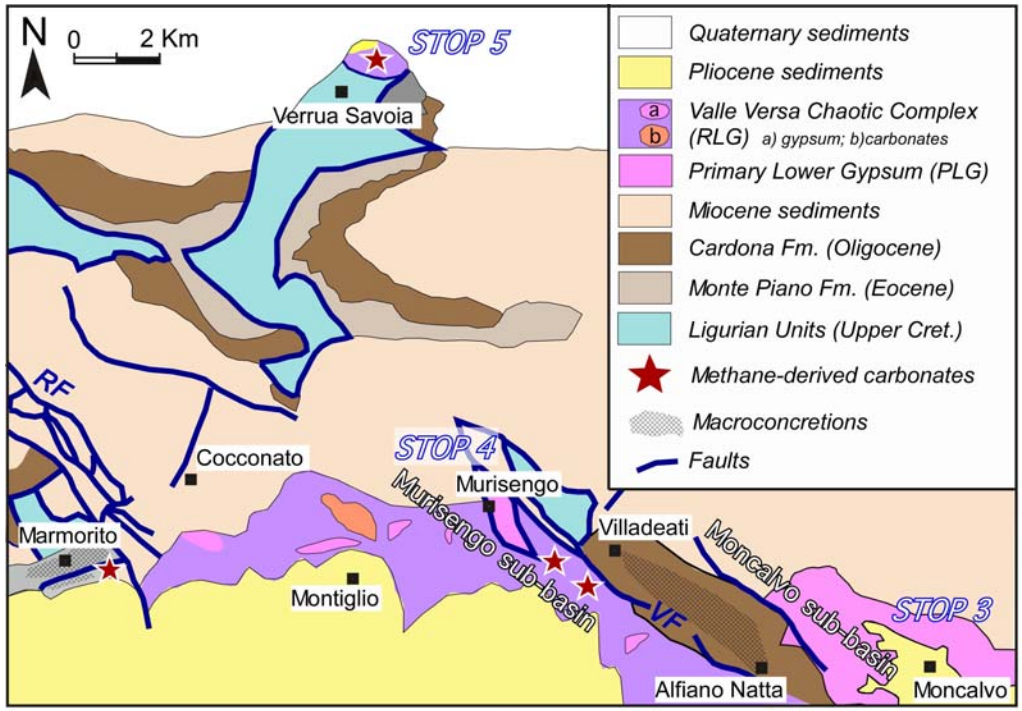

The Moncalvo sub-basin

At Moncalvo, the Messinian deposits are exposed in the local quarry mostly developed in the underground. This succession was previously interpreted as a huge block enclosed into the Valle Versa chaotic complex (Dela Pierre et al., 2003). However, the recent study of the underground quarry

Fig. 21 - Simplified geological map of the Monferrato (modified from Dela Pierre et al., 2003). Location in Fig. 4A. **RF:** Rio Freddo fault zone; **VF:** Villadeati fault.

DOI: 10.3301/GFT.2016.03

and of three cores drilled in the surroundings showed that *in situ* primary evaporites (PLG unit) are actually preserved there, deformed in an open NW-SE anticline. The PLG unit overlies the Sant'Agata Fossili marls and is followed by the Cassano Spinola conglomerates, through an erosional unconformity that cuts progressively towards the NE, *i.e.* towards the basin margin.

Topmost part of the Sant'Agata Fossili marls

A core drilled in the quarry allowed us to study the transition from the Sant'Agata Fossili marls to the PLG unit. Four shale/marl cycles were observed in the topmost part and studied for their fossil content (foraminifers and calcareous nannofossils) (Fig 22). Regular fluctuations of types and abundance of foraminifers in the shaley and the marly hemicycles confirm that the lithologic cyclicity reflects precession-driven climate changes. The foraminifer assemblages are dominated by benthic forms, even though plankton is very common to abundant in some layers. The planktonic assemblage is dominated by opportunistic species living in surface (*Globigerinita glutinata*, *Turborotalita multiloba*, *T. quinqueloba*) or intermediate waters (*Globigerina bulloides*, *Globigerinella pseudobesa*, *G. obesa*, *N. acostaensis*, *Orbulina* spp.). These taxa suggest a eutrophic unstable water column with broad seasonal variations (Hallock et al., 1991). Benthic assemblage is dominated by infaunal taxa (*B. echinata*, *Brizalina dilatata*, *B. spathulata*) suggesting low oxygen availability and high fluxes of organic matter at the sea floor; epifaunal taxa (*Hanzawaia boueana*, *Cibicidoides* spp.) are less abundant. Shallow water taxa (*Cibicides* spp., *Discorbis* spp., *Elphidium* spp., *Glabratella* spp., *Rosalina* spp. and rare *Ammonia beccarii*) are present, rather more common in cycle Mm2. This assemblage suggests deposition in outer neritic environment (circalittoral zone), close to a coastal area (Bernardi, 2013). The Messinian marker *Globorotalia miotumida* is not present; however, the recovery of *N. acostaensis* with dominant right coiled specimens, of *T. multiloba* and the strong impoverishment of the foraminiferal assemblage allow recognition of subzone MM13ic (Lourens et al., 2004). In the calcareous nannofossil assemblages, reliable biostratigraphic markers (such as *Amaurolithus* spp. and *Discoaster* spp.) are absent, due to the proximal location of the section. The last recovery of foraminifers and calcareous nannofossils is recorded in the lower part of cycle Mm3 (Fig. 22): the barren part of the section is referable to the "Non distinctive zone" (Iaccarino, 1985). Calcareous nannofossil analysis evidences a sharp *S. abies* abundance peak in cycle Mm3. In the same cycle minor but significant peaks of *H. carteri* and *R. clavigera* are found, as in the Pollenzo section in cycle Pm5 (Lozar, unpublished data), thus allowing the direct correlation to the Pollenzo section. This oligospecific

DOI: 10.3301/GFT.2016.03

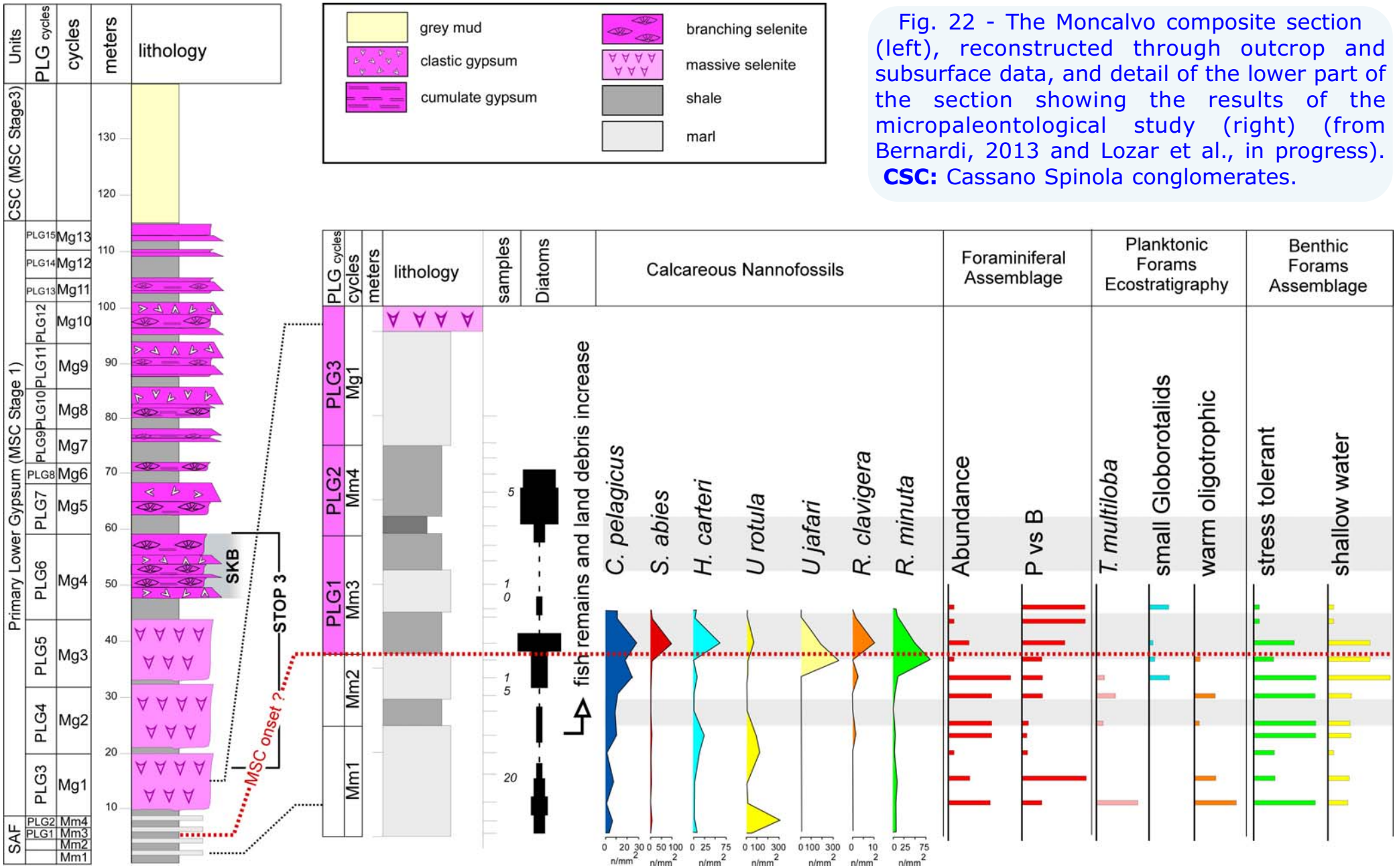

Fig. 22 - The Moncalvo composite section (left), reconstructed through outcrop and subsurface data, and detail of the lower part of the section showing the results of the micropaleontological study (right) (from Bernardi, 2013 and Lozar et al., in progress). **CSC:** Cassano Spinola conglomerates.

DOI: 10.3301/GFT.2016.03

assemblage testifies the presence of deteriorated enivironmental conditions and strong salinity fluctuations. Sponge spicules and diatoms are increasingly common from cycle Mm1 to cycle Mm4. As already suggested in the Pollenzo section, we tentatively place the onset of the MSC in cycle Mm3, where the *S. abies* abundance peak occurs. As a consequence, the upper two cycles of the Sant'Agata Fossili marls at Moncalvo are interpreted as the lateral equivalent of cycles PLG1 and PLG2 and the first local gypsum bed correlates to cycle PLG3; this correlation also confirms that the first occurrence of the branching selenite facies correlates to PLG6 in the PB.

The PLG unit

Integration of outcrop and subsurface data allowed to recognise 13 lithologic cycles (Mg1-Mg13), truncated at the top by the erosional unconformity at the base of the post-evaporitic Cassano Spinola conglomerates (Fig. 22). Thick (up to 10 m) massive selenite beds characterises the lowermost three cycles (Fig. 23A). They are composed of vertically oriented crystals (Fig. 23B) whose size varies through the beds, indicating variation of the saturation conditions of the brines, from less saturated (larger crystals) to more saturated (smaller crystals) conditions. The re-entrant angles of the crystals are rich in clay particles, suggesting a terrigenous flux from a nearby emerged source area. Sparse filamentous fossils are also present ("spaghetti-like structure") (Figs. 23C, D), which were interpreted as remains of sulphide-oxidizing bacteria (Dela Pierre et al., 2015).

A sharp facies change is observed from the fourth local cycle (Mg4) upwards, marked by the appearance of the branching selenite facies and cumulate gypsum (Fig. 23E). Layers of clastic gypsum, commonly marked by a lower sharp erosional boundary (Fig. 23E), are interbedded to the primary evaporites, suggesting the erosion of penecontemporaneous selenite layers originally placed at the margins of the Moncalvo sub-basin. Bed Mg4 shows a total thickness of 10 m and is correlated to the Sturani-key bed (= PLG6) (Fig. 22). This correlation is supported by biostratigraphic data, according to which the first gypsum layer (Mg1) should correspond to cycle PLG3, being the uppermost two cycles of the Sant'Agata Fossili marls the lateral equivalents of cycles PLG1 and PLG2. Bed Mg5 (= PLG7) shows analogous features but minor thickness. In the quarry, bed Mg5 is unconformably overlaid by the Cassano Spinola conglomerates, which are very poorly exposed. However, additional eight cycles (Mg6-Mg13) were observed beneath this last unit in the two cores drilled in the SE of the quarry, suggesting that the erosional unconformity at the base of the CSC cuts and progressively deepens towards the NW. These upper cycles are characterised by thinner gypsum beds (max. 2 m) and thicker shaly layers as already noted in the Pollenzo section.

DOI: 10.3301/GFT.2016.03

Fig. 23 - **A)** Panoramic view of the Moncalvo quarry. **B)** A twinned selenite crystals in bed Mg3. Note the turbid core, related to the presence of solid inclusions. **C)** Detail of B, showing mm-thick laminae in the re-entrant angle of the crystal. **D)** Detail of C: the solid inclusions consist of clay and sparse curved filaments. **E)** The Sturani key-bed in the underground quarry: the primary evaporites consist of cumulate gypsum (cg) and branching selenite (bs). A layer of clastic gypsum (CG), containing dm-sized marly clasts is recognisable. The base is sharp and erosional.

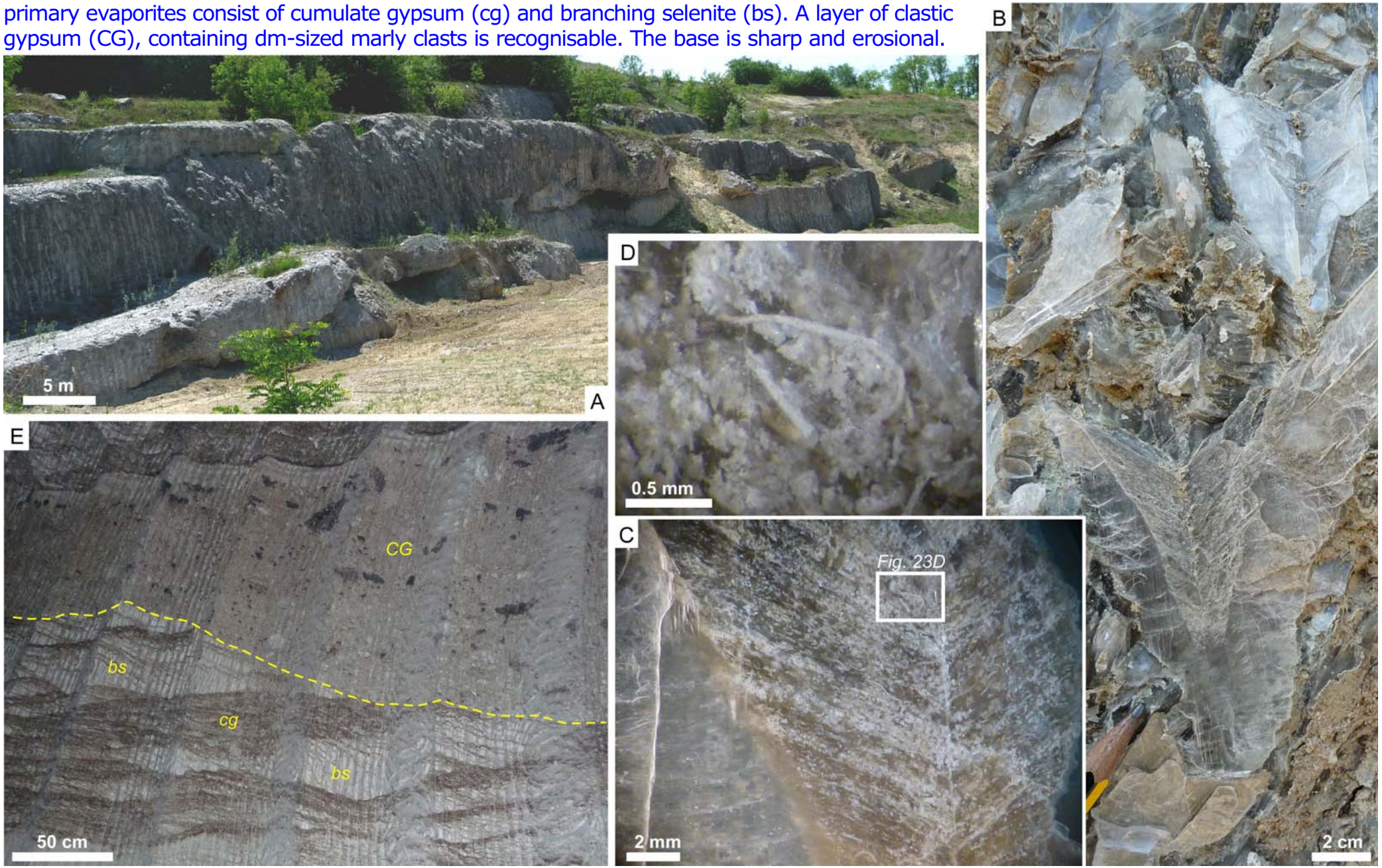

DOI: 10.3301/GFT.2016.03

The Murisengo sub-basin

This sub-basin is bordered by the Villadeati and Rio Freddo fault zones, to the E and W respectively (Fig. 21). No *in situ* primary evaporites were observed in the outcrop and the MSC succession is represented by the Valle Versa chaotic complex (VVC), corresponding to the RLG unit (Dela Pierre et al., 2011) and deposited during stage 2 of the MSC. Inadequate outcrop conditions did not allow to observe the basal surface of these deposits. However, geological mapping indicates that it corresponds to an angular unconformity separating the chaotic unit from Tortonian/early Messinian (Sant'Agata Fossili marls), or even older (the Oligocene Cardona fm.) sediments. The thickness of the exposed VVC is about 200 m but, according to seismic data, it reaches a thickness of 400 m in the buried depocentres (Savigliano-Alessandra basins).
The VVC consists of blocks of gypsum and carbonate rocks embedded in a poorly exposed fine-grained matrix. The latter is made up of silty muds enclosing mm- to m-sized marly clasts derived from Messinian and pre-Messinian units. Gypsum blocks originated from the PLG unit, not preserved *in situ* in the Murisengo sub-basin; the largest ones, up to hundreds of metres in size, retain the cyclic successions of clayey and bottom-grown selenite layers. Layers of clastic gypsum (gypsrudites and gypsarenites) are also present. Locally (Banengo quarry), the transition from the pre-evaporitic marine sediments and the lower four PLG cycles is preserved within a large block, although strongly deformed.
Carbonate rocks form metre-sized blocks and consists of two main types: 1) skeletal grainstones and packstones, interpreted as remnants of a pre-MSC (?) carbonate platform whose original location is unknown (Dela Pierre et al., 2002); 2) methane-derived carbonates. These rocks have been found in the proximity of the main tectonic structures, *i.e.* along the Villadeati and Rio Freddo faults (Clari et al., 2009) and at the northern edge of the Monferrato, close to the Padane thrust front (Verrua Savoia quarry) (Fig. 21). The carbonate cements of these rocks show negative $\delta^{13}C$ values, suggesting that carbonate precipitation was induced by microbial oxidation of methane (Clari et al., 2004; 2009). The best outcrop is the Verrua Savoia quarry, that exposes a chaotic succession interpreted as the geological record of a Messinian mud volcano (see below).

Interpretation of the VVC

The VVC has been interpreted as the product of large scale mass wasting events triggered by the intra-Messinian tectonic activity. This caused the southward tilting of the Monferrato in response of the northward propagation of the Padane thrust front (Dela Pierre et al., 2007). The emplacement of the chaotic unit was associated to the

DOI: 10.3301/GFT.2016.03

upward rising of methane-rich fluids and shale diapirism along the main tectonic discontinuities, possibly triggered by gas hydrate destabilisation (Clari et al., 2009; Natalicchio et al., 2013). These processes, documented in the same time interval in other Mediterranean areas (Iadanza et al., 2013), were responsible for the formation of authigenic methane-derived carbonates and locally of mud volcano edifices (Verrua Savoia).

STOP 3 - The Murisengo quarry: the Valle Versa chaotic complex.

Warning: to visit this stop contact the owner of the quarry

This Stop is located in an underground quarry (Fig. 24A) close to the Villadeati fault and set in the VVC (Fig. 21). Gypsum blocks, ranging in size from few metres up to several tens of metres are exposed (Fig. 24B), together with layers of clastic gypsum (gypsrudites and gypsarenites; Fig. 24C) and a fine-grained matrix. The latter includes mm- to m-sized marly clasts and clay chips, some of which sourced from the lower Messinian Sant'Agata Fossili marls (Fig. 24D). In the largest blocks, cyclic successions of the PLG unit are preserved (Fig. 24B). In particular, we will observe a block formed by four cycles. The single gypsum layers are up to ten metres thick and are composed of massive selenite, passing upward to banded selenite. At the base of these layers, beautiful nucleation cones can be observed.

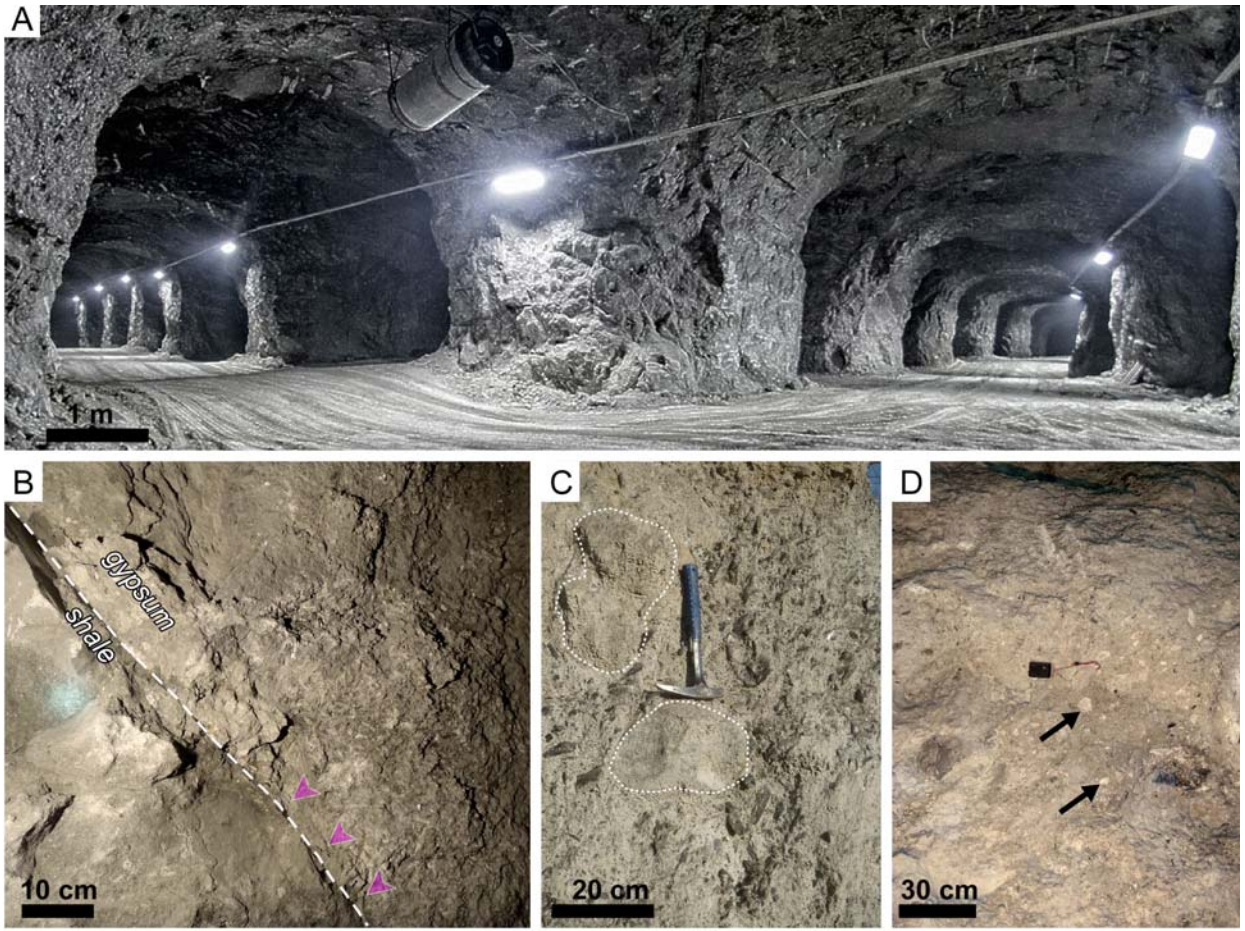

Fig. 24 – **A)** The Murisengo underground quarry. **B)** The transition from a shaly and a gypsum layer, preserved in a large block. **C)** A layer of clastic gypsum, including clasts of twinned selenite crystals, and two dm-sized blocks of laminated gypsum (white dotted lines). **D)** The matrix of the VVC. The arrows point to whitish marly clast.

DOI: 10.3301/GFT.2016.03

STOP 4 - The Verrua Savoia quarry

The Verrua Savoia quarry exposes a chaotic succession ascribed to the VVC (Clari et al., 2004). This chaotic succession is overlaid by Pliocene deposits of the Argille Azzurre Fm (Figs. 25, 26A). This quarry is now a protected geosite, equipped with explanation panels (Zunino et al., 2012).

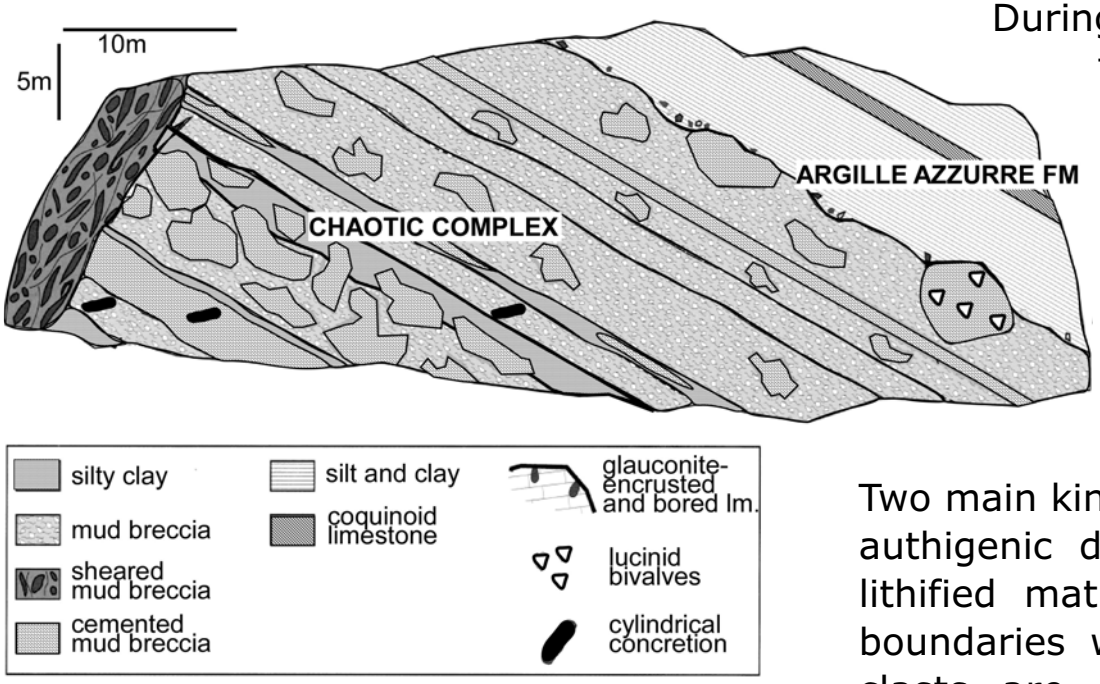

Fig. 25 – Schematic cross section of the upper part of the VVC as exposed in the Verrua Savoia quarry in 2004 (modified from Clari et al., 2004).

During quarry activity, soft mud breccias with a sheared textures (Figs. 25, 26E) were observed, intruding the chaotic complex (Fig. 25). Unfortunately, these relationships cannot be observed nowadays, because of the modification of quarry front and extensive weathering of the outcrop. More resistant masses of carbonate-cemented rocks originally enclosed within the soft breccias are however still observable, both in place and accumulated on the quarry front (Figs. 25, 26A). Two main kinds of rocks can be distinguished, both cemented by authigenic dolomite: 1) dm- to m-sized masses of strongly lithified matrix-supported breccias, showing sharp or diffuse boundaries with the host unlithified breccias (Fig. 26A). The clasts are composed of planktonic foraminifer-rich marly wackestone, sourced from the underlying Miocene succession. The cemented masses show similar structure and composition of the encasing soft mud breccias, but different degree of lithification. Clusters of articulated and disarticulated bivalve shells of the chemosymbiotic taxon *Lucina* sp. are present (Fig. 26D). 2) Cylindrical concretions, made up of light coloured marly limestones, that are about 10 cm in diameter and more than 1 m long (Fig. 26B). They crosscut the bedding planes at high angles and show rounded smoothed edges. The axial portion of the concretions may be empty, or more commonly filled with sediments (Fig. 26C).

DOI: 10.3301/GFT.2016.03

Fig. 26 - **A)** Panoramic view of the Verrua Savoia quarry: large cemented masses are recognisable. **B)** Cylindrical concretions (arrows) cross cutting the bedding planes at high angle. **C)** Polished slab of a cylindrical concretion, showing the axial portion filled with dark sediment. **D)** Detail of a cemented block. Moulds of the chemosymbiotic bivalve *Lucina* sp. are recognisable (arrows). **E)** Unconsolidated mud breccias with clear sheared texture.

DOI: 10.3301/GFT.2016.03

The intergranular cement of both kind of rocks is mainly dolomite, characterised by low $\delta^{13}C$ values (from –23 to –10 ‰ PDB) and $\delta^{18}O$ values up to +7 ‰ PDB. The $\delta^{13}C$ values testify carbonate precipitation induced by microbial oxidation of methane, whereas the markedly positive $\delta^{18}O$ signature, ubiquitous in the cylindrical concretions, is possibly the evidence for the destabilisation of gas hydrates (Clari et al., 2004; 2009).

The upper boundary between the chaotic succession and the overlying Pliocene deposits is a sharp erosional surface underlined by a lag of glauconite-stained silty clay clasts. This surface locally becomes highly irregular because of the presence of boulder-sized bodies of *Lucina*-bearing breccias described above (Fig. 25). The upper and lateral surfaces of these masses are bored. Centimetre-long *Trypanites*-like boring are recognisable, which are filled with phosphatised and glauconitized sediments. Glauconite is also present as thin crusts on the same surfaces.

Clari et al. (2004) have interpreted the chaotic succession exposed at Verrua Savoia as the geological record of a Messinian mud volcano, on the basis of comparison with present-day examples. Viscous mud and semilithified clasts sourced by the underlying sedimentary succession testify short paroxistic phases, when unconsolidated mud breccias were erupted from the mud volcano crater and flowed along its flanks (Fig. 27A). Long periods of quiescence led to the localized cementation of the mud breccias, and their colonization by chemosymbiotic bivalves because

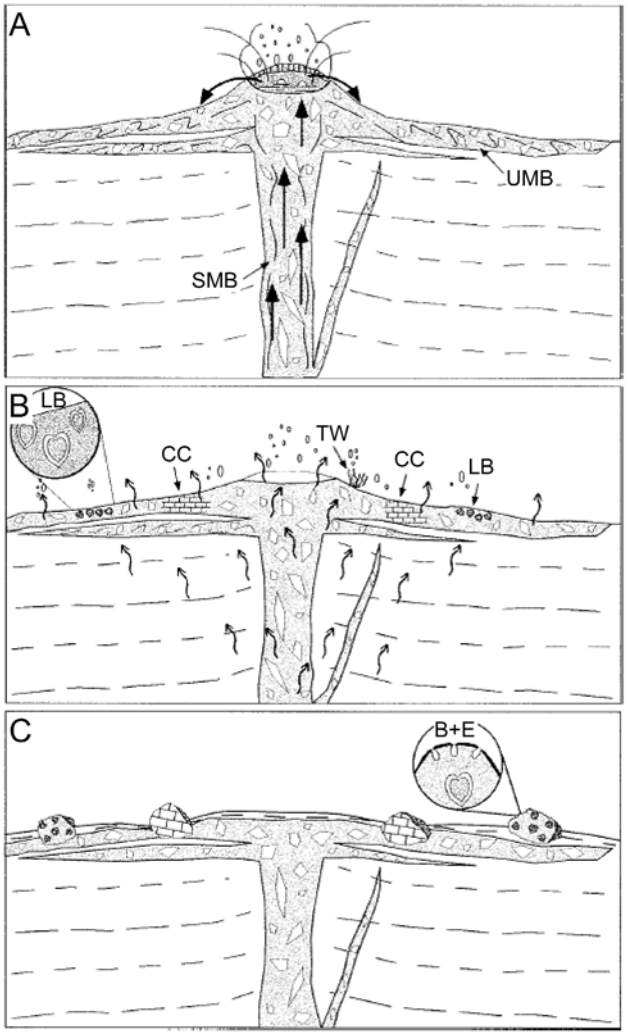

Fig. 27 - Schematic cartoon showing different phases of the activity of the submerged mud volcano (from Clari et al., 2004). **A)** During short periods of paroxysmal activity, the eruption of a mud volcano gives origin to an irregular cone-shaped edifice consisting of unsheared mud breccias (UMB). Sheared mud breccias (SMB) are formed in the conduit. **B)** Long periods of quiescence are characterized by slow and diffuse degassing. Colonies of chemosymbiotic taxa settle and live around the seeps. In this phase, carbonate precipitation linked to microbial degradation of methane locally occurs (CC, carbonate cementation; TW, tube worms; LB, lucinid bivalves). **C)** The extinction of a mud volcano is followed by the partial destruction of the cone-shaped edifice (B+E: boring and encrustations).

DOI: 10.3301/GFT.2016.03

of the persisting slow-rate expulsion of methane-rich fluids through all the mud volcano edifice (Fig. 27B). The cylindrical concretions represent instead the plumbing system of the mud volcano (for modern analogous, see Diaz del Rio et al., 2003) due to the localized cementation of portions of the flanks of the mud volcano edifice. Boring and glauconite crusts at the external surface of the cemented masses indicate that they were exhumed and exposed at the sea floor at the end of mud volcano activity, immediately prior to deposition of Pliocene marine sediments (Fig. 27C).

The Pliocene sediments: micropaleontological data

The Pliocene succession is represented by about 80 meters of well stratified marly clays, silts and sandy silts, affected by faults, with interbedded sand and calcarenite banks, progressively more frequent and thicker upwards (Dela Pierre et al., 2003; Violanti, 2012). Only sandy silts, sands and calcarenites are represented in the upper transect. Foraminiferal preservation was generally poor, tests were encrusted or partially included in calcareous aggregates. Reworked tests, of Eocene forms in the lower section, and of Miocene to lower Pliocene taxa in the middle and upper layers, are abundant. Planktonic foraminiferal assemblages are mainly given by Miocene to Pliocene taxa such as *Globoturborotalita decoraperta, Globigerinoides obliquus, Globigerinoides extremus* and less common *N. acostaensis*. The lower part of the marly clays and silts was correlated to the MPl3 Zone, on the co-occurrence of *Globorotalia margaritae* and *Globorotalia puncticulata*, the following sandy silts and calcarenites, yielding *G. puncticulata* and *G. puncticulata padana*, to the MPl4a Zone. The reasonably *in situ* (not reworked) benthic foraminiferal assemblages of the Verrua Savoia silts are very diversified and yield common deep outer neritic to bathyal taxa (*Anomalinoides helicinus, Cassidulina carinata, Cibicidoides pseudoungerianus, Hoeglundina elegans, Planulina ariminensis, Siphonina reticulata, Uvigerina peregrina, U. rutila*) (Van Morkhoven et al., 1986). The infaunal, stress tolerant *Bolivina spp.*, *Brizalina* spp. and *Bulimina* spp., preferential of muddy sediments, are scarce. In the uppermost sands and calcarenites inner neritic taxa (*Elphidium* spp., *Neoconorbina terquemi* and *Cibicides* spp.) are dominant, documenting the basin shallowing.

ACKNOWLEDGEMENTS

We would like to thanks Fassa Bortolo and Estrazione Gesso and in particular Alberto Gianotti and Sandro Gennaro for allowing us to visit and study the Moncalvo and Murisengo gypsum quarries. Research funded by University of Torino grants 2013 and 2014 to FD.

DOI: 10.3301/GFT.2016.03

DOI: 10.3301/GFT.2016.03

References

Aloisi G., Pierre C., Rouchy J.M., Foucher J.P., Woodside J. & Party M.S. (2000) - Methane-related authigenic carbonates of eastern Mediterranean Sea mud volcanoes and their possible relation to gas hydrate destabilisation. Earth and Planetary Science Letters, 184, 321-338.

Baker P.A. & Kastner M. (1981) - Constraints on the formation of sedimentary dolomite. Science, 213, 214-216.

Bailey J.V., Orphan V.J., Joye S.B. & Corsetti F. (2009) - Chemotrophic microbial mats and their potential for preservation in the rock record. Astrobiology, 9, 1-17.

Bellanca A., Caruso A., Ferruzza G., Neri R., Rouchy J.M., Sprovieri M. & Blanc-Valleron M.M. (2001) - Sedimentary record of the transition from marine to hypersaline conditions in the Messinian Tripoli Formation in the marginal areas of the Sicilian Basin. Sedimentary Geology, 140, 87-106.

Bernardi E. (2013) - Integrated stratigraphy of the northernmost record of the Messinian salinity crisis: new insights from the Tertiary Piedmont Basin. PhD thesis, University of Torino, 184 pp.

Bertotti G. & Mosca P. (2009) - Late orogenic vertical movements within the arc of the SW Alps and Ligurian Alps. Tectonophysics, 475, 117-127.

Bigi G., Cosentino D., Parotto M., Sartori R. & Scandone P. (1990) - Structural Model of Italy. Geodinamic Project: Consiglio Nazionale delle Ricerche, S.EL.CA, scale 1:500,000, sheet 1.

Blanc-Valleron M.M., Pierre C., Caulet J.P., Caruso A., Rouchy J.M., Cespuglio G., Sprovieri R., Pestrea S. & Di Stefano E. (2002) - Sedimentary, stable isotope and micropaleontological records of paleoceanographic change in the Messinian Tripoli Formation (Sicily, Italy). Palaeogeography, Palaeoclimatology, Palaeoecology, 185, 255-286.

Brunner B., Bernasconi S.M., Kleikemper J. & Schroth M.H. (2005) - A model for oxygen and sulfur isotope fractionation in sulfate during bacterial sulfate reduction processes. Geochimica et Cosmochimica Acta, 69, 4773-4785.

Carnevale G., Landini W. & Sarti G. (2006) - Mare versus Lago-mare. Marine fishes and the Mediterranean environment at the end of the Messinian Salinity Crisis. Journal of the Geological Society, London, 163, 75-80.

Carnevale G., Longinelli A., Caputo D., Barbieri M. & Landini W. (2008) - Did the Mediterranean marine reflooding precede the Mio-Pliocene boundary? Paleontological and geochemical evidence from upper Messinian sequences of Tuscany, Italy. Palaeogeography, Palaeoclimatology, Paleoecology, 257, 81-105.

CIESM (2008) - The Messinian Salinity Crisis from mega-deposits to microbiology – A consensus report. CIESM Workshop Monographs N° 33, F. Briand Eds, Monaco, pp. 168.

Cita M.B., Wright R.C., Ryan W.B.F. & Longinelli A. (1978) - Messinian paleoenvironments, In: Hsü, K.J., Montadert, L. et al. (Eds.), Initial Reports of the Deep Sea Drilling Project 42. U.S. Government Printing Office, Washington D.C, 1003-1035.

Clari P., Dela Pierre F., Novaretti A. & Timpanelli M. (1995) - Late Oligocene-Miocene sedimentary evolution of the critical Alps-Apennine junction: the Monferrato area, Northwestern Italy. Terra Nova, 7, 144-152.

Clari P., Cavagna S., Martire L. & Hunziker J. (2004) - A Miocene mud volcano and its plumbing system: a Chaotic complex revisited. Journal of Sedimentary Research, 74, 662-676.

DOI: 10.3301/GFT.2016.03

Clari P., Dela Pierre F., Martire L. & Cavagna S. (2009) - The Cenozoic CH4-derived carbonates of Monferrato (NW Italy): a solid evidence of fluid circulation in the sedimentary column. Marine Geology, 265, 167-184.

Colombero S., Bonelli E., Kotsakis T., Pavia G., Pavia M. & Carnevale G. (2013) - Late Messinian rodents from Verduno (Piedmont, NW Italy): biochronological, palaeoecological and palaeobiogeographic implications. Geobios, 46, 111-125.

Colombero S., Angelone C., Bonelli E., Carnevale G., Cavallo O., Delfino M., Giuntelli P., Pavia G., Pavia M., Repetto G. & Mazza P. (2014) - The upper Messinian assemblages of fossil vertebrate remains of Verduno (NW Italy): Another brick for a latest Miocene bridge across the Mediterranean. Neues Jahrbuch für Geologie und Paläontologie, Abhandlungen, 272, 287-324.

De Lange G.J. & Krijgsman W. (2010) - Messinian salinity crisis: a novel unifying shallow gypsum/deep dolomite formation mechanism. Marine Geology, 275, 273-277.

Dela Pierre F., Clari P., Cavagna S. & Bicchi E. (2002) - The Parona chaotic complex: a puzzling record of the Messinian (Late Miocene) events in Monferrato (NW Italy). Sedimentary Geology, 152, 289-311.

Dela Pierre F., Piana F., Fioraso G., Boano P., Bicchi E., Forno M.G., Violanti D., Balestro G., Clari P., d'Atri A., De Luca D., Morelli M. & Ruffini R. - (2003). Note illustrative della Carta Geologica d'Italia alla scala 1:50.000, Foglio 157 Trino. APAT, 1-147.

Dela Pierre F., Festa A. & Irace A. (2007) - Interaction of tectonic, sedimentary and diapiric processes in the origin of chaotic sediments: an example from the Messinian of Torino Hill (Tertiary Piedmont Basin, northwestern Italy). Geological Society of America Bulletin, 119, 1107-1119.

Dela Pierre F., Martire L., Natalicchio M., Clari P. & Petrea C. (2010) - Authigenic carbonates in the upper Miocene sediments of the Tertiary Piedmont Basin (NW Italy): vestiges of an ancient gas hydrate stability zone? Geological Society of America Bulletin, 122, 994-1010.

Dela Pierre F., Bernardi E., Cavagna S., Clari P., Gennari R., Irace A., Lozar F., Lugli S., Manzi V., Natalicchio M., Roveri M. & Violanti, D. (2011) - The record of the Messinian salinity crisis in the Tertiary Piedmont Basin (NW Italy): The Alba section revisited. Palaeogeography, Palaeoclimatology, Palaeoecology, 310, 238-255.

Dela Pierre F., Clari P., Bernardi E., Natalicchio M., Costa E., Cavagna S., Lozar F., Lugli S., Manzi V., Roveri M. & Violanti D. (2012) - Messinian carbonate-rich beds of the Tertiary Piedmont Basin (NW Italy): microbially-mediated products straddling the onset of the salinity crisis. Palaeogeography, Palaeoclimatology, Palaeoecology, 344-345, 78-93.

Dela Pierre F., Clari P., Natalicchio M., Ferrando S., Giustetto, R., Lozar F., Lugli S., Manzi V., Roveri M. & Violanti D. (2014) - Flocculent layers and bacterial mats in the mudstone interbeds of the Primary Lower Gypsum Unit (Tertiary Piedmont Basin, NW Italy): Archives of palaeoenvironmental changes during the Messinian salinity crisis. Marine Geology, 355, 71-87.

Dela Pierre F., Natalicchio M., Ferrando S., Giustetto R., Birgel D., Carnevale G., Gier S., Lozar F., Marabello D. & Peckmann J. (2015) – Are the large filamentous microfossils preserved in Messinian gypsum colorless sulfide-oxidizing bacteria?. Geology, 43, 855-858.

Diaz del Rio V., Somoza L., Martin-Frias J., Mata M.P., Delgado A., Hernandez-Molina F.J., Lunar R., Martin-Rubi J.A., Maestro A., Fernadez-Puga M.C., Leon R., Llave E., Medialdea T. & Vazquez J.T. (2003) - Vast fields of hydrocarbon-derived carbonate chimneys related to the accretionary wedge/olistostrome of the Gulf of Cadiz. Marine Geology, 195, 177-200.

Di Stefano A. & Sturiale G.(2010) - Refinements of calcareous nannofossil biostratigraphy at the Miocene/Pliocene Boundary in the Mediterranean region. Geobios, 43, 5-20.

DOI: 10.3301/GFT.2016.03

Di Stefano E., Sprovieri R. & Scarantino S. (1996) - Chronology of biostratigraphic events at the base of the Pliocene. Palaeopelagos, 6, 401-414.

Flores J.A., Sierro F.J., Filippelli G.M., Barcena M.A., Perez-Folgado M., Vazquez A. & Utrilla R. (2005) - Surface water dynamics and phytoplankton communities during deposition of cyclic late Messinian sapropel sequences in the western Mediterranean. Marine Micropaleontology, 56, 50-79.

Gallardo V.A. (1977) - Large benthic microbial communities in sulphide biota under Peru-Chile subsurface counter current. Nature, 286, 331-332.

Gaudant J. & Cavallo O. (2008) - The Tortonian-Messinian fish faunas of Piedmont (Italy) and the Adriatic trough: a synthesis dedicated to the memory of Carlo Sturani (1938-1975). Bollettino Società Paleontologica Italiana, 47, 177-189.

Gibbs S., Shackleton N. & Young J.R. (2004) - Orbitally forced climate signals in mid-Pliocene nannofossil assemblages. Marine Micropaleontology, 51, 39-56.

Grossi F., Gliozzi E. & Cosentino D. (2011) - Paratethyan ostracod immigrants mark the biostratigraphy of the Messinian Salinity Crisis. Joannea Geologie und Palaeontologie, 11, 66-68.

Guido A., Jacob J., Gautret P., Laggoun-Defarge F., Mastandrea A. & Russo F. (2007) - Molecular fossils and other organic markers as paleoenvironmental indicators of the Messinian Calcare di Base Formation: Normal versus stressed marine deposition (Rossano Basin, northern Calabria, Italy). Palaeogeography, Palaeoclimatology, Palaeoecology, 255, 265-283.

Hallock P., Premoli Silva I. & Boersma A. (1991) - Similarities between planktonic and larger foraminiferal evolutionary trends through Paleogene paleoceanography changes. Palaeogeography, Palaeoclimatology, Palaeoecology, 83, 49-64.

Hendry J.P., Pearson M.J., Trewin N.H. & Fallick A.E. (2006) - Jurassic septarian concretions from NW Scotland record interdependent bacterial, physical and chemical processes of marine mudrock diagenesis. Sedimentology, 53, 537-565.

Hilgen F.J. & Krijgsman W. (1999) - Cyclostratigraphy and astrochronology of the Tripoli diatomite Formation (pre-evaporite Messinian, Sicily, Italy). Terra Nova 11, 16-22.

Hsü K.J., Cita M.B. & Ryan W.B.F. (1973) - The origin of the Mediterranean evaporites. In: Ryan, W.B.F., Hsü, K.J., et al. (Eds.), Initial Report of Deep Sea Drilling Program 13. U.S. Government Printing Office, Washington DC, pp. 1203-1231.

Kastner M. (1984) - Sedimentology: control of dolomite formation. Nature, 5985, 410-411.

Kennett J.P. & Srinivasan M.S. (1983) - Neogene planktonic foraminifera. Hutchinson Ross Publ. Comp., Stroudsburg, 265 pp.

Krijgsman W., Hilgen F.J., Raffi I., Sierro F.J. & Wilson D.S. (1999) - Chronology, causes and progression of the Messinian salinity crisis. Nature, 400, 652-655.

Krijgsman W., Fortuin A.R., Hilgen F.J., Roep T.B. & Sierro F.J. (2001) - Astrochronology for the Messinian Sorbas Basin (SE Spain) and orbital (precessional) forcing for evaporite cyclicity. Sedimentary Geology, 140, 43-60.

Krijgsman W., Blanc-Valleron M.M., Flecker R., Hilgen F.J., Kouwenhoven T.J., Merle D., Orzsag-Sperber F. & Rouchy J.-M. (2002) - The onset of the Messinian salinity crisis in the Eastern Mediterranean (Pissouri Basin, Cyprus). Earth Planetary Science Letters 194/3-4, 299-310.

Kouwenhoven T.J., Morigi C., Negri A., Giunta S., Krijgsman W. & Rouchy J.M. (2006) - Palaeoenvironmental evolution of the eastern Mediterranean during the Messinian: constraints from integrated microfossil data of the Pissouri Basin (Cyprus). Marine Micropalaeontology, 60, 17-44.

DOI: 10.3301/GFT.2016.03

Iaccarino S. (1985) - Mediterranean Miocene and Pliocene planktic Foraminifera, In: Bolli, H. M., Saunders, J. B., Perch-Nielsen, K., (Eds.), Plankton Stratigraphy. Cambridge University Press, Cambridge, 283-314.

Iadanza A., Sampalmieri G., Cipollari P., Mola M. & Cosentino D. (2013) - The "Brecciated Limestones" of Maiella, Italy: rheological implications of hydrocarbon-charged fluid migration in the Messinian Mediterranean Basin. Palaeogeography, Palaeoclimatology, Palaeoecology, 390, 130-147.

Irace A., Clemente P., Natalicchio M., Ossella L., Trenkwalder S., De Luca D. A., Mosca P., Piana F., Polino R. & Violanti D. (2010) - Geologia e idrostratigrafia profonda della Pianura Padana occidentale: La Nuova Lito Firenze, pp. 110, ISBN 978-88-904554-0-7.

Jannasch H.W., Nelson D.C. & Wirsen C.O. (1989) - Massive natural occurrence of unusually large bacteria (*Beggiatoa* spp.) at a hydrothermal deep-sea vent site. Nature, 342, 834-836.

Laskar J., Robutel P., Joutel F., Gastineau M., Correia A. & Levrard B. (2004) - A long-term numerical solution for the insolation quantities of the Earth. Astronomy and Astrophysics, 428, 261-285.

Lozar F., Violanti D., Dela Pierre F., Bernardi E., Cavagna S., Clari P., Irace A., Martinetto E. & Trenkwalder S. (2010) - Calcareous nannofossils and foraminifers herald the Messinian salinity crisis: the Pollenzo section (Alba, Cuneo; NW Italy). Geobios, 43, 21-32.

Lourens L., Hilgen F., Shackleton N.J., Laskar J. & Wilson D. (2004) - The Neogene period, In: Gradstein, F.M., Ogg, J.G., Smith, A.G., (Eds.), A geologic time scale 2004. Cambridge University Press, 409-440.

Lugli S., Schreiber B.C. & Triberti B. (1999) - Giant polygons in the Realmonte mine (Agrigento, Sicily): evidence for the desiccation of a Messinian halite basin. Journal of Sedimentary Research, 69, 764–771.

Lugli S., Bassetti M.A., Manzi V., Barbieri M., Longinelli A. & Roveri M. (2007) - The Messinian 'Vena del Gesso' evaporites revisited: characterization of isotopic composition and organic matter. In: Schreiber B.C., Lugli S., Bąbel M., (Eds), Evaporites Through Space and Time. Geological Society of London, Special Publication, 285, 143-154.

Lugli S., Manzi V., Roveri M. & Schreiber B.C. (2010) - The Primary Lower Gypsum in the Mediterranean: a new facies interpretation for the first stage of the Messinian salinity crisis. Palaeogeography, Palaeoclimatology, Palaeoecology, 297, 83-99.

Manzi V., Roveri M., Gennari R., Bertini A., Biffi U., Giunta S., Iaccarino S., Lanci L., Lugli S., Negri A., Riva A., Rossi M.E. & Taviani M. (2007) - The deep-water counterpart of the Messinian Lower Evaporites in the Apennine foredeep: the Fanantello section (Northern Apennines, Italy). Palaeogeography, Palaeoclimatology, Palaeoecology, 251, 470-499.

Manzi V., Lugli S., Roveri M. & Schreiber B.C. (2009) - A new facies model for the Upper Gypsum of Sicily (Italy): chronological and palaeoenvironmental constraints for the Messinian salinity crisis in the Mediterranean. Sedimentology, 56, 1937-1960.

Manzi V., Gennari R., Hilgen F., Krijgsman W., Lugli S., Roveri M. & Sierro F.J. (2013) - Age refinement of the Messinian salinity crisis onset in the Mediterranean. Terra Nova, 25, 315-322.

Mc Kenzie J.A., Jenkyns H.C. & Bennet G.G. (1979) - Stable isotope study of the cyclic diatomite claystones from the Tripoli Formation, Sicily: a prelude to the Messinian Salinity Crisis. Palaeogeography, Palaeoclimatology, Palaeoecology, 29, 125-141.

Møeller M.M., Nielsen L.P. & Jørgensen B.B. (1985) – Oxygen response and mat formation by *Beggiatoa* spp.. Applied and Environmental Microbiology, 252, 166-173.

Mosca P., Polino R., Rogledi S. & Rossi M. (2009) - New data for the kinematic interpretation of the Alps–Apennines junction (Northwestern Italy). International Journal of Earth Sciences, 99, 833-429.

DOI: 10.3301/GFT.2016.03

Natalicchio M., Birgel D., Dela Pierre F., Martire L., Clari P., Spötl C. & Peckmann J. (2012) - Polyphasic carbonate precipitation in the shallow subsurface: insights from microbially-formed authigenic carbonate beds in upper Miocene sediments of the Tertiary Piedmont Basin (NW Italy). Palaeogeography, Palaeoclimatology, Palaeoecology, 329/330, 158-172.

Natalicchio M., Dela Pierre F., Clari P., Birgel D., Cavagna S., Martire L. & Peckmann J. (2013) - Hydrocarbon seepage during the Messinian salinity crisis in the Tertiary Piedmont Basin (NW Italy). Palaeogeography, Palaeoclimatology, Palaeoecology, 390, 68-80.

Natalicchio M., Dela Pierre F., Lugli S., Lowenstein T.K, Feiner S. J., Ferrando S., Manzi V., Roveri M. & Clari P. (2014) - Did late Miocene (Messinian) gypsum precipitate from evaporated marine brines? Insight from the Piedmont Basin (Italy). Geology, 42, 179-182.

Oliveri E., Neri R., Bellanca A.& Riding R. (2010) - Carbonate stromatolites from a Messinian hypersaline setting in the Caltanissetta Basin, Sicily: petrographic evidence of microbial activity and related stable isotope and rare earth element signature. Sedimentology, 47, 142-161.

Orszag-Sperber F. (2006) - Changing perspectives in the concept of Lago-Mare" in Mediterranean Late Miocene evolution. Sedimentary Geology, 188/189, 259-277.

Orszag-Sperber F., Caruso A., Blanc-Valleron M.M., Merle D. & Rouchy J.M. (2009) - The onset of the Messinian salinity crisis: insights from Cyprus sections. Sedimentary Geology, 217, 52-64.

Panieri G., Lugli S., Manzi V., Roveri M., Schreiber C.B. & Palinska K.A. (2010) - Ribosomal RNA gene fragments from fossilized cyanobacteria identified in primary gypsum from the late Miocene, Italy. Geobiology, 8, 101-111.

Peckmann J. & Thiel V. (2004) - Carbon cycling at ancient methane-seeps. Chemical Geology, 205, 443-467.

Piana F. (2000) - Structural features of Western Monferrato (Alps-Apennines junction zone, NW Italy). Tectonics, 19, 943-960.

Pierre C. & Rouchy J.M. (2004) - Isotopic compositions of diagenetic dolomites in the Tortonian marls of the Western Mediterranean margins: evidence of past gas hydrate formation and dissociation. Chemical Geology 205, 469-484.

Raffi I., Mozzato C., Fornaciari E., Hilgen F.J. & Rio D. (2003) - Late Miocene calcareous nannofossil biostratigraphy and astrochronology for the Mediterranean region. Micropaleontology, 49, 1-26.

Roberts H.H. & Aharon P. (1994) - Hydrocarbon-derived carbonate buildups of the northern Gulf of Mexico continental slope: a review of submersible investigations. Geo-Marine Letters, 14, 135-148.

Rossi M., Mosca P., Polino R. & Biffi U. (2009) - New outcrop and subsurface data in the Tertiary Piedmont Basin (NW Italy): unconformity bounded stratigraphic units and their relationships with basin modification phases. Rivista Italiana di Paleontologia e Stratigrafia, 115, 305-335.

Rouchy J.M. & Caruso A. (2006) - The Messinian Salinity Crisis in the Mediterranean basin: a reassessment of data and an integrated scenario. Sedimentary Geology, 188/189, 35-67.

Rouchy J.M. & Monty C.L. (1981) - Stromatolites and cryptalgal laminites associated with Messinian gypsum of Cyprus. In: Monty C.L. (Ed.), Phanaerozoic stromatolites. Springer Verlag, 155-178.

Roure F., Bergerat F., Damotte B., Mugnier J.L. & Polino R. (1996) - The ECORS-CROP Alpine seismic traverse. Bulletin de la Société Géologique de France, 170, 1-113.

Roveri M., Lugli S., Manzi V. & Schreiber B.C. (2008) - The Messinian Sicilian stratigraphy revisited: new insights for the Messinian Salinity Crisis. Terra Nova, 20, 483-488.

DOI: 10.3301/GFT.2016.03

Roveri M., Flecker R., Krijgsman W., Lofi J., Lugli S., Manzi V., Sierro F. J., Bertini A., Camerlenghi A., de Lange G.J., Govers R., Hilgen F.J., Hübscher C., Meijer P.T. & Stoica M. (2014) - The Messinian Salinity Crisis: Past and future of a great challenge for marine sciences. Marine Geology, 352, 25-58.

Ryan W.B.F. (2009) - Decoding the Messinian salinity crisis. Sedimentology, 56, 95-136.

Sass E., Bein A. & Almogi-Labin A. (1991) - Oxygen-isotope composition of diagenetic calcite in organic-rich rocks: evidence for ^{18}O depletion in marine anaerobic pore water. Geology, 19, 839-842.

Sahling H., Rickert D., Raymond W. L. Linke P. & Suess E. (2002) - Macrofaunal community structure and sulfide flux at gas hydrate deposits from the Cascadia convergent margin, NE Pacific. Marine Ecology Progress Series, 231, 121-138.

Sánchez-Román M., McKenzie J.A., Rebello Wagener A. de L., Rivadeneyra M. & Vasconcelos C. (2009) - Presence of sulfate does not inhibit low-temperature dolomite precipitation. Earth and Planetary Science Letters 285, 131-139.

Schulz H.N., Brinkhoff T., Ferdelman G., Hernandez Marine M., Teske A. & Jørgensen B.B. (1999) - Dense populations of a giant sulfur bacterium in Namibian shelf sediments. Science, 284, 493-495.

Schulz H.N. & Jørgensen B.B. (2001) - Big bacteria. Annual Review of Microbiology, 55, 105-137.

Sierro F.J., Krijgsman W., Hilgen F.J. & Flores J.A. (2001) - The Abad composite (SE Spain): a Mediterranean reference section for the Messinian and the Astronomical Polarity Time Scale (APTS). Palaeogeography, Palaeoclimatology, Palaeoecology, 168, 143–172.

Sierro F.J., Flores J.A., Francés G., Vazquez A., Utrilla R., Zamarreño I., Erlenkeuser H. & Barcena M.A. (2003) - Orbitally controlled oscillations in planktic communities and cyclic changes in western Mediterranean hydrography during the Messinian. Palaeogeography, Palaeoclimatology, Palaeoecology, 190, 289-316.

Sturani C. (1973) - A fossil eel (*Anguilla* sp.) from the Messinian of Alba (Tertiary Piedmont Basin). Palaeoenvironmental and palaeogeographic implications. In: Messinian events in the Mediterranean. K. Nederl. Akad. Wetensch., Amsterdam, 243-255.

Sturani C. (1976) - Messinian facies in the Piedmont basin. Memorie Società Geologica Italiana 16, 11-25.

Sturani C. & Sampò M. (1973) - Il Messiniano inferiore in facies diatomitica nel Bacino Terziario Piemontese. Memorie Società Geologica Italiana 12, 335-338.

Teichert B.M.A., Bohrmann G. & Suess E. (2005) - Chemoherms on Hydrate Ridge - Unique microbially-mediated carbonate buildups growing into the water column. Palaeogeography, Palaeoclimatology, Palaeoecology, 227, 67-85.

Vai G.B. & Ricci Lucchi F. (1977) - Algal crusts, autochtonous and clastic gypsum in a cannibalistic evaporite basin; a case history from the Messinian of Northern Apennine. Sedimentology, 24, 211-244.

Van Morkhoven F.P.C.M., Berggren W.A. & Edwards A.S. (1986) - Cenozoic Cosmopolitan Deep-Water Benthic Foraminifera. Centres Recherches Exploration-Production Elf-Aquitaine Bulletin, 11, 421 pp.

Violanti D. (2012) - Pliocene Mediterranean Foraminiferal Biostratigraphy: A Synthesis and Application to the Paleoenvironmental Evolution of Northwestern Italy. In: Elitok Ö. (Ed.). Stratigraphic Analysis of Layered Deposits, InTech, Rjecka, 123-160.

Violanti D., Trenkwalder S., Lozar F. & Gallo L.M. (2009) - Micropalaeontological analyses of the Narzole core: biostratigraphy and palaeoenvironment of the late Messinian and early Zanclean of Piedmont (Northwestern Italy). Bollettino Società Paleontologica Italiana, 48, 167-181.

Violanti D., Dela Pierre F., Trenkwalder S., Lozar F., Clari P., Irace A. & d'Atri A. (2011) - Biostratigraphic and palaeoenvironmental analyses of the Messinian/Zanclean boundary and Zanclean succession in the Moncucco quarry (Piedmont, northwestern Italy).

DOI: 10.3301/GFT.2016.03

Bulletin Société Géologique de France, 182, 149-162.

Violanti D., Lozar F., Dela Pierre F., Natalicchio M., Bernardi E., Clari P. & Cavagna S. (2013) - Stress tolerant microfossils of a Messinian succession from the northern Mediterranean basin (Pollenzo section, Piedmont, Northwestern Italy). Bollettino Società Paleontologica Italiana, 52, 45-54.

Wortmann U.G., Chernyavsky B., Bernasconi S.M., Brunner B., Boettcher M.E. & Swart P.K. (2007) - Oxygen isotope biogeochemistry of pore water sulfate in the deep biosphere: dominance of isotope exchange reactions with ambient water during microbial sulfate reduction (ODP Site 1130). Geochimica et Cosmochimica Acta, 71, 4221-4232.

Wright D.T. & Oren A. (2005) - Nonphotosynthetic bacteria and the formation of carbonates and evaporites through time. Geomicrobiology Journal, 22, 27-53.

Zunino M., Cavagna S., Clari P. & Pavia G. (2012) - Two examples of the geoheritage potential of Piedmont (NW Italy): Verrua Savoia for the present, Valle Ceppi for the future. Geoheritage, 4/3, 165-175.

DOI: 10.3301/GFT.2016.03